Journal of Energy Chemistry 94 (2024) 340–356

Contents lists available at ScienceDirect

Journal of Energy Chemistry

journal homepage: www.elsevier.com/locate/jechem

http://www.journals.elsevier.com/journal-of-energy-chemistry/

Review

Decoupled water electrolysis: Flexible strategy for pure hydrogen production with small voltage inputs

Kexin Zhou [a], Jiahui Huang [a], Daili Xiang [a], Aijiao Deng [c], Jialei Du [a,*], Hong Liu [a,b,*]

[a] Institute for Advanced Interdisciplinary Research (iAIR), Collaborative Innovation Center of Technology and Equipment for Biological Diagnosis and Therapy in Universities of Shandong, University of Jinan, Jinan 250022, Shandong, China
[b] State Key Laboratory of Crystal Materials, Shandong University, Jinan 250100, Shandong, China
[c] Zhengzhou Vocational College of Industrial Safety, Zhengzhou 451192, Henan, China

ARTICLE INFO

Article history:
Received 29 January 2024
Revised 2 March 2024
Accepted 6 March 2024
Available online 16 March 2024

Keywords:
Hydrogen production
Conventional water splitting
Decoupled water splitting
Redox mediators
Biomimetics

ABSTRACT

Hydrogen gas is widely regarded as an ideal green energy carrier and a potential alternative to fossil fuels for coping with the aggravating energy crisis and environmental pollution. Currently, the vast majority of the world's hydrogen is produced by reforming fossil fuels; however, this hydrogen-making technology is not sustainable or environmentally friendly because of its high energy consumption and large carbon emissions. Renewables-driven water splitting ($2H_2O \rightarrow 2H_2 + O_2$) becomes an extensively studied scheme for sustainable hydrogen production. Conventional water electrolysis requires an input voltage higher than 1.23 V and forms a gas mixture of H_2/O_2, which results in high electricity consumption, potential safety hazards, and harmful reactive oxygen species. By virtue of the auxiliary redox mediators (RMs) as the robust H^+/e^- reservoir, decoupled electrolysis splits water at a much lower potential and evolves O_2 ($H_2O + RMs_{ox} \rightarrow O_2 + H\text{-}RMs_{red}$) and H_2 ($H\text{-}RMs_{red} \rightarrow H_2 + RMs_{ox}$) at separate times, rates, and spaces, thus producing the pure target hydrogen gas safely. Decoupled electrolysis has accelerated the development of water electrolysis technology for H_2 production. However, it is still lack of a comprehensive and in-depth review in this field based on different types of RMs. This review highlights the basic principles and critical progress of this emerging water electrolysis mode over the past decade. Several representative examples are then displayed in detail according to the differences in the RMs. The rational choice and design of RMs have also been emphasized. Subsequently, novel applications of decoupled water splitting are briefly discussed, including the manufacture of valuable chemicals, Cl_2 production, pollutant degradation, and other half-reactions in artificial photosynthesis. Finally, the key characteristics and disadvantages of each type of mediator are summarized in depth. In addition, we present an outlook for future directions in decoupled water splitting. Thus, the flexibility in the design of mediators provides huge space for improving this electrochemical technology.
© 2024 Science Press and Dalian Institute of Chemical Physics, Chinese Academy of Sciences. Published by ELSEVIER B.V. and Science Press. All rights reserved.



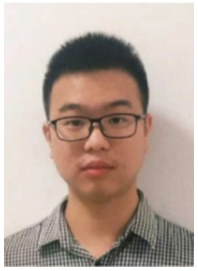
Kexin Zhou is currently a graduate student in the Institute for Advanced Interdisciplinary Research (iAIR) at University of Jinan. Her research subject focuses on electrocatalytic water splitting for hydrogen production.



Jiahui Huang is currently a graduate student in the Institute for Advanced Interdisciplinary Research (iAIR) at University of Jinan. His research subject focuses on electro-upgrading of waste plastics for co-production of green H_2 and valued chemicals.

* Corresponding authors.
E-mail addresses: ifc_dujl@ujn.edu.cn (J. Du), hongliu@sdu.edu.cn (H. Liu).

https://doi.org/10.1016/j.jechem.2024.03.001
2095-4956/© 2024 Science Press and Dalian Institute of Chemical Physics, Chinese Academy of Sciences. Published by ELSEVIER B.V. and Science Press. All rights reserved.



Daili Xiang is currently a graduate student in the Institute for Advanced Interdisciplinary Research (iAIR) at University of Jinan. His research subject focuses on electrochemical H_2 production coupled with biomass upgrading.



Aijiao Deng got her master degree at Hunan Normal University in 2015. Now she is a lecture at Zhengzhou Vocational College of Industrial Safety. Her research subject focuses on the design of novel nanomaterials and electrochemical cells for energy transformation and storage.



Jialei Du completed his Ph.D. degree at Tongji University in 2017. Now, he is an associate professor in the Institute for Advanced Interdisciplinary Research (iAIR), University of Jinan. His research interests mainly cover unconventional water splitting, organic electrosynthesis, and integrated electrodes.



Hong Liu is a professor in State Key Laboratory of Crystal Materials, Shandong University. He received his Ph.D. degree from Shandong University in 2001. His current research is mainly focused on chemical processing of nanomaterials for energy-related applications, including photo- and electro-catalysis, tissue engineering, especially the interaction between stem cell and nanostructure of biomaterials, as well as the nonlinear optical crystals.

1. Introduction

The survival and development of human beings are undoubtedly inseparable from abundant energy, rich resources, and a healthy environment. Population explosions and economic growth have led to an increase in energy demand and severe environmental crises. By far, traditional fossil fuels (e.g., coal, petroleum, and natural gas) still accounts for the largest proportion of the current energy structure [1–3]. However, they are nonrenewable and are gradually being depleted, and serious environmental pollution has been caused by their exploitation and utilization [4,5]. These issues could be handled by exploring green and inexhaustible energy sources to replace fossil fuels [6–9].

Among the numerous new energy sources, hydrogen gas has long been advocated as an ideal energy vector owing to its many remarkable characteristics, including diverse applications, high calorific value (285.8 kJ/mol), storability, transportability, carbon neutrality, renewability, and cleanliness (i.e., the sole product of its combustion is clean water in a fuel cell) [10]. It is noteworthy that hydrogen gas is rarely found in its pure form in nature [11]. The reforming of fossil fuels represents the current mainstream pathway for global hydrogen production; however, it is neither sustainable nor environmentally friendly because of its high energy consumption and tremendous carbon emissions [12]. Thus, developing economical, sustainable and biological friendly technology for green hydrogen production is highly desirable to accelerate society's transition to a hydrogen economy.

Nowadays, renewable energy-driven electrolytic water splitting ($2H_2O \rightarrow 2H_2 + O_2$, E° = 1.23 V vs. NHE) is a promising strategy for green H_2 mass production obviating carbon-based fossil resources [13–19]. Thus, the invested electricity can be derived from renewable yet intermittent and diffuse energy sources, such as sunlight, hydropower, tides, and wind. The electricity obtained is then converted into stable chemical energy (hydrogen bonds) via electrolysis, implying that hydrogen enables storing surplus electrical energy [20,21]. Hydrogen generated through water electrolysis accounts for only 4% of global hydrogen production [19].

In conventional water splitting, the target hydrogen gas is produced at the cathode, and oxygen gas is simultaneously generated at the anode. Therefore, the desired hydrogen evolution reaction (HER) is strictly coupled with the kinetically sluggish oxygen evolution reaction (OER), resulting in the concurrent formation of two gases ($H_2 + O_2$). The protons and energetic electrons released from the OER are directly employed to make H_2 [22]. However, a high electrical energy input (E > 1.23 V) and extra voltage (overpotentials) is typically required for this one-step water splitting process (OER + HER), which increases the power cost of hydrogen production (> 4.5 kWh m^{-3} H_2) [23–26] and could place severe constraints on the wide application of this technology. The utilization of an added ion exchange membrane or salt bridge would increase the internal resistance between the catalytic electrodes, even though they can prevent the two half-reactions from occurring in the same electrolytic cell to a certain extent [27]. In addition, unstable energy inputs are difficult to efficiently utilize for decomposing water [28]. The service life of the exchange membrane may be shortened by the harmful reactive oxygen species (e.g., $O_2^{\cdot-}$, H_2O_2, •OH, and •OOH), which are formed on account of the coexistence of H_2, O_2, and electrocatalysts [29,30]. Furthermore, a potential safety hazard exists owing to the formation of an explosive H_2/O_2 mixed gas (the explosion limit of H_2 in O_2 is only 4 mol%) [31]. In addition, the economic value of H_2 is directly related to its purity, which would be negatively affected by the unavoidable crossover of the two gases [32,33]. Together, H_2 large-scale production from water electrolysis presents enormous difficulties in practical applications.

The innovation of electrolysis mode has been an efficient route for promoting the development of water electrolysis to maximize the return of energy investment[34], such as field-assisted water splitting [35,36], self-powered water splitting [37,38], hybrid water splitting [39–41], tandem water splitting [42–44], high/low-temperature water splitting [45,46], seawater splitting [47,48], and chemical looping water splitting [49]. In 2013, Cronin's et al. first proposed a decoupled strategy to solve those issues associated with conventional water electrolysis [50]. According to their design concept, the overall water splitting is spatiotemporally separated into two isolated steps; therefore, the HER and OER are not directly interrelated, and pure hydrogen can be produced with the aid of a liquid redox mediator. Thereafter, extensive efforts have been devoted to exploring new decoupled water electrolysis systems and their applications to meet future hydrogen energy needs and other areas (Fig. 1). Over the past 10 years, significant progress has been made in this field [51–57]. Decoupled water

splitting has considerable prospects for development. However, comprehensive reviews based on the different types of redox mediators are lacking.

In this review, we provide a detailed discussion of several representative redox relays for this emerging decoupled technology. Metal oxyhydroxides/hydroxides and benzoquinones/phenols are identified as common intermediates in this decoupled process. In addition, the operating principles, strengths, and weaknesses of these redox couples are highlighted. Subsequently, the idea of designing innovative decoupling agents is emphasized. Finally, we comprehensively analyze the underlying constraints and development prospects for redox-mediated water splitting.

2. Basic principle of decoupled electrolysis

During natural photosynthesis, water molecules ($2H_2O \rightarrow O_2 + 4H^+ + 4e^-$) are mildly oxidized at the $CaMn_4O_5$ cluster of the oxygen-evolving complex in photosynthesis II under light irradiation [58–60]. The evolved oxygen gas is vented into the atmosphere and is vital for respiration and metabolism in humans, animals, and plants. The generated protons and electrons (i.e., reductive equivalents) are transported and employed to reduce nicotinamide adenine dinucleotide phosphate ($NADP^+$) to NADPH, which then releases protons and electrons during the transformation of CO_2 in the atmosphere into high-energy carbohydrates via a series of enzymatic catalysis in photosynthesis I. Meanwhile, the NADPH itself returns to its original $NADP^+$ (Fig. 2a) [61–63]. From a certain point of view, water molecules can be regarded as the H^+/e^- source for CO_2 fixation. $NADP^+$/NADPH can shuttle protons and electrons for subsequent CO_2 reduction; therefore, it can be considered as a redox mediator. The OER and CO_2 reduction are not directly coupled but are connected with the $NADP^+$/NADPH redox couple. Overall, CO_2 fixation in nature is not a one-step half-reaction but a sequential one. This natural decoupling process provides a significant opportunity to improve the performance of traditional electrocatalytic water decomposition devices.

Based on the concept of biomimetics, decoupled water splitting was creatively disclosed by Cronin et al. in 2013 for electrolytic hydrogen production in acidic media [50] (Fig. 2b). In the proposed decoupled method, full water splitting can be divided into two separate sub-reactions via the introduction of redox mediator. As illustrated in Fig. 2(c and d), the OER is firstly paired with the reduction of mediator ($H_2O + RMs_{ox} \rightarrow O_2 + H\text{-}RMs_{red}$). The electrons and protons released from the OER are temporarily buffered by the third mediator. The HER is then matched with the reoxidation of the reduced mediator ($H\text{-}RMs_{red} \rightarrow H_2 + RMs_{ox}$). The reversible redox wave of the mediator lies between the onsets of the OER and HER (Fig. 2c). Therefore, the OER and HER can occur at different times and in different spaces. The rates of these two half-reactions are not connected to each other. Formally, water molecules are split into the constituent gases O_2 and H_2, and these two gases are liberated successively. The desired high quantity of green hydrogen can be produced at lower potentials using this decoupled system in the absence of expensive membranes, and the mediators maintain their original structures [51–57].

This decoupled strategy can effectively resolve the aforementioned concerns in conventional water splitting and even provide a new scheme for hydrogen storage. These non-innocent redox mediators can store and transport electrons and/or protons, thus having functions similar to natural $NADP^+$/NADPH. Over the past ten years, a large variety of polyoxometalates [50,64–71], quinone derivatives [72–76], battery electrodes [27,77–112], metal complexes [113–116], redox flow batteries [117–120], and others [121–126] have been successfully exploited as external redox mediators for decoupled water splitting (Fig. 3). The efficiency of a decoupled electrolysis system is strongly related to the physicochemical properties of redox mediators. They usually exhibit suitable redox potentials (Fig. 2c), perfect cycle stability, good redox reversibility (Fig. 2c), high H^+/e^- storage capacity, fast kinetics, and good solubility in aqueous media.

3. Redox mediators for decoupled electrolysis

The selection and design of low-cost redox mediators are crucial for constructing decoupled water electrolysis systems for H_2 production on demand. This section discusses the decoupling process for water electrolysis according to the different types of redox mediators. Table S1 (see Supporting Information) summarizes some key metrics (e.g., redox potentials, solutions of operation, decoupling mechanism, and stability) of the redox mediators discussed in this review.

3.1. Polyoxometalates

Polyoxometalates are among the most important inorganic nanomaterials and have been deployed in numerous areas, such as heterogeneous catalysis, energy conversion, environmental protection, and energy storage [127]. It has the main features of general complexes and metal oxides and a strong storage capacity for electrons and protons [69,128]. Molecular polyoxometalates were first used for decoupled electrocatalytic hydrogen liberation [50]. Commercial $H_3PMo_{12}O_{40}$ [50,65,66], $H_4SiW_{12}O_{40}$ [64,67,71], and as-prepared $H_6ZnW_{12}O_{40}$ [70] were successively developed by Cro-

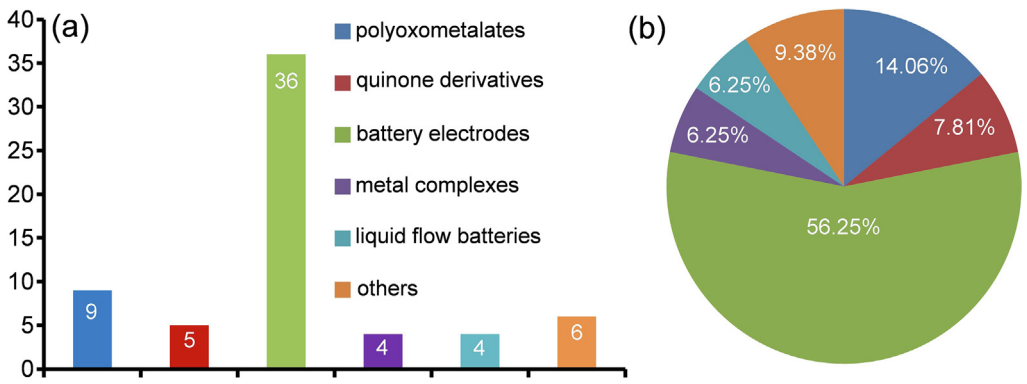


Fig. 1. The number (a) and proportion (b) of published papers about decoupled water splitting using different redox mediators during 2013–2023.

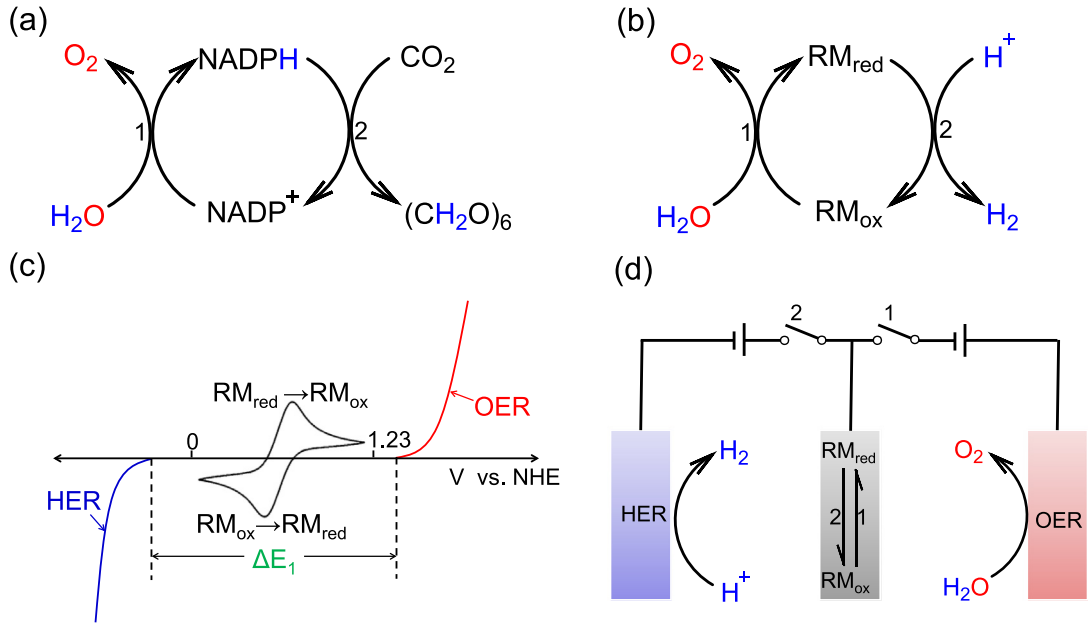


Fig. 2. (a) OER and CO_2 reduction in natural photosynthesis. (b) OER and HER in decoupled water splitting. RM represents redox mediator. (c) Linear sweep voltammetries (LSVs) for OER and HER, cyclic voltammetry (CV) for redox mediator. ΔE_1 represents the actual voltage for water splitting. (d) The schematic illustration of decoupled water splitting for the double-step hydrogen production.

nin's group as all-inorganic electron-coupled proton buffers (ECPBs) for decoupled water electrolysis.

Considering $H_3PMo_{12}O_{40}$ as an example, the protons and electrons donated by the anodic OER are used for the protonation and reduction of the phosphomolybdic-type ECPB (Fig. 4a). Subsequently, the power polarity was reversed, and the reduced state (ECPB*) of the polyoxometalates was reoxidized for the next cycle, yielding protons and electrons for the cathodic HER (Fig. 4b). Electrochemical tests demonstrate that the redox peaks of ECPB are exactly in the HER and OER starting potential ranges (Fig. 4c). ECPB reduction occurred preferentially over HER (Fig. 4d), and ECPB* was considerably easier to oxidize than water (Fig. 4e). The pH of the electrolyte remained unaltered, which was attributed to the good buffering ability of ECPB. As shown in Fig. 4(d and e), two lower voltages were required to split water to independently give H_2 (1.23 V) and O_2 (1.71 V) at a current density of 100 mA/cm^2. Nevertheless, the combined voltage required by this decoupled system (2.94 V) is higher than that of the conventional proton exchange membrane water electrolyzer (PEMWE, 2.55 V); therefore, the maximum efficiency of the two-step water splitting system is approximately 87% relative to the PEMWE, which is due to the high overpotential of ECPB oxidation/reduction. Full Faradaic efficiency was observed for H_2 generation via decoupled electrolysis using this mediator. Obviously, O_2 and H_2 were released stepwise in the same chamber using $H_3PMo_{12}O_{40}$ as the mediator for decoupled water electrolysis. Interestingly, solar power can be adopted for powering decoupled water splitting in the presence of polyoxometalates with zero electrochemical bias, promoting sporadic and fluctuating power-to-gas conversion [65,66].

Silicotungstic acid ($H_4SiW_{12}O_{40}$) has been introduced as a recyclable redox mediator for hydrogen production via tandem electrochemical-chemical catalysis [64]. CV measurements validated that $H_4SiW_{12}O_{40}$ was reduced in preference to the HER with glassy carbon (GC) as the working electrode (Fig. 5a). In the first step, O_2 was evolved at the anode via water oxidation, and the released electrons and protons were used to reduce $H_4SiW_{12}O_{40}$ to $H_6SiW_{12}O_{40}$ at the cathode. This reduced silicotungstic species was then transferred outside the electrolyzer to react with the platinum catalyst, spontaneously generating gaseous H_2 (Fig. 5b). O_2 and H_2 are successively released in distinct chambers via the decoupled system, eliminating the formation of high-pressure gases inside the electrolytic cell, which largely cause membrane degradation and gas crossover in conventional PEMWE. Furthermore, the H_2 production rate in this decoupled system is more than 30 times faster than that of the state-of-the-art PEMWE (Fig. 5c, red data). Large amounts of H_2 are released when $H_6SiW_{12}O_{40}$ is exposed to the Pt catalyst (Fig. 5d). The overall energy efficiency of this mediated system (63%) is comparable to that of room-temperature PEMWE (67%). And the redox potential of $H_5SiW_{12}O_{40}/H_4SiW_{12}O_{40}$ is just 0.01 V vs. NHE (Fig. 5a), which is close to that of HER, so it has low reducing ability towards protons, and only 45%–60% of the hydrogen is collected. The yield of hydrogen gas can be increased by introducing organic solvents [129]. The catalytic evolution of hydrogen from reduced silicotungstic acid can also be achieved using earth abundant materials [67,68]. In addition, this silicotungstic cluster has been reported to mediate decoupled hydrogen production over a wide range of current densities (25–500 mA cm^{-2}) in a proton exchange membrane cell [71].

As for the polyoxometalates-assisted hydrogen production, polyoxometalates must be dissolved in aqueous solutions at a low pH to maintain adequate protonation of their reduced states. Because polyoxometalates are commonly in high-valence states, O_2 is first produced. A robust proton exchange membrane is essential for selectively permeating protons, but polyoxometalates are not. Electrochemical cycling tests and UV-vis spectra measurements show that the dissolved polyoxometalates can be reduced and re-oxidized several times without apparent degradation (within 4%), which imply they have prolonged stability and good redox reversibility [50,64]. The molecular weights (MWs) of these metal oxides are huge (for example, $H_3PMo_{12}O_{40}$, MW > 1800 g mol^{-1}; $H_4SiW_{12}O_{40}$, MW > 2800 g mol^{-1}), and they can accept only $2H^+/2e^-$; thereby their storage capacity is minimal, which increases the frequency of alternating reduction–oxidation cycles. Even after 10 years of development, the materials used in this domain are still rare.

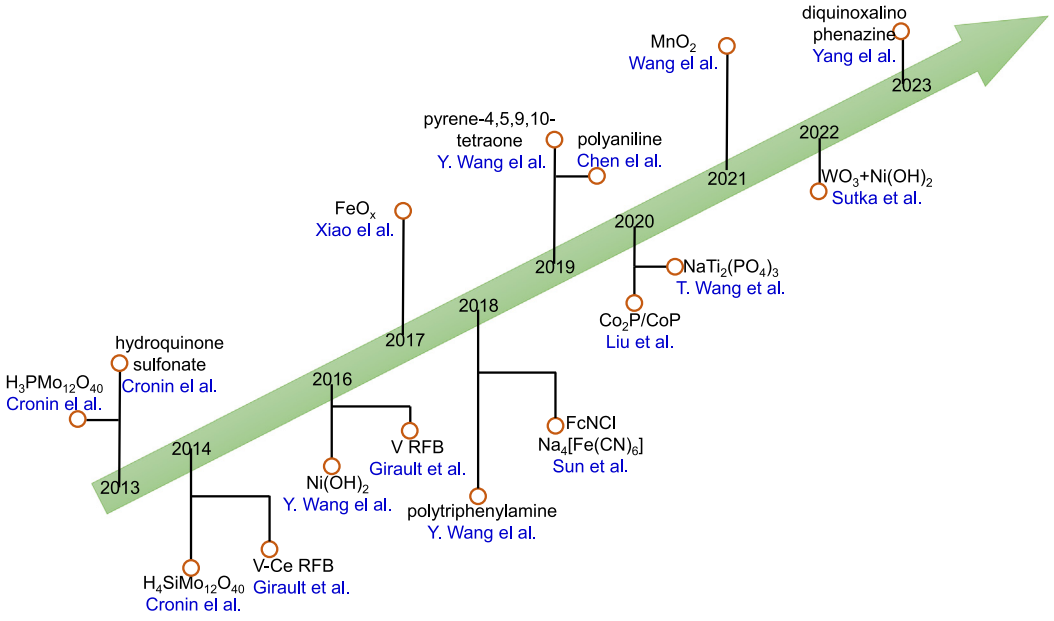


Fig. 3. The representative redox mediators for decoupled water splitting. RFB and FcNCl represent redox flow battery and (ferrocenylmethyl)trimethylammonium chloride, respectively.

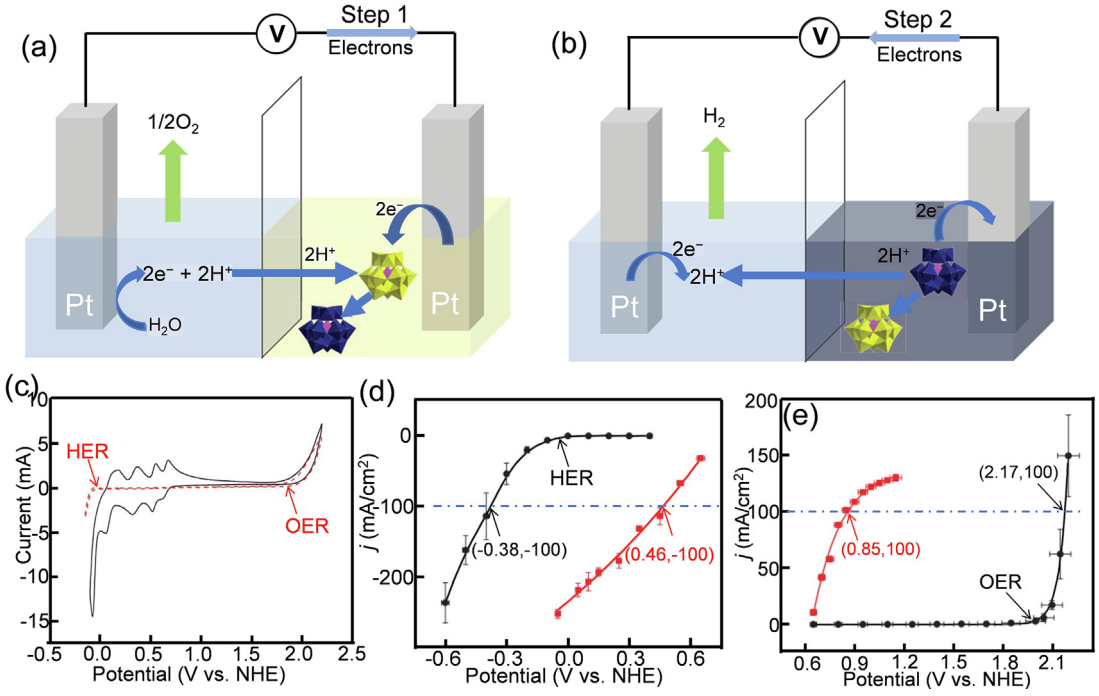


Fig. 4. (a and b) Schematic of the ECPB-based approach to decoupled water splitting. (c) CVs of 0.5 M phosphomolybdic acid (solid black) and 1.0 M H_3PO_4 (dashed red). (d and e) Current-voltage curves for the reduction (d) and oxidation (e) of 1.0 M H_3PO_4 solution with (red) and without (black) ECPB/ECPB* mixture. Reproduced with permission from Ref. [50]. Copyright 2013, Nature.

3.2. (Hydro)quinones

(Hydro)quinone derivatives have been identified as intermediate redox reservoirs that aid water oxidation during natural photosynthesis [130]. Inspired by this natural process, several organic quinone compounds (Fig. 6a) with low molecular weight, good stability, strong redox reversibility, and high water solubility have recently been exploited as biomimetic mediators for decoupled hydrogen generation [72–76]. Their mechanism of storing H^+/e^- is predominantly based on the reversible conversion between quinone and hydroquinone (i.e., C=O/C−OH), which is also inseparable from the strongly acidic environment. Furthermore, their water solubility can be attributed to additional hydrophilic functional groups (i.e., sulfonate).

In 2013, Cronin et al. pioneered an important study on commercially available hydroquinone sulfonate functioning as an organic small-molecule ECPB to completely separate the two half-reactions of water electrolysis (Fig. 6b) [72]. Fig. 6(c and d) evince

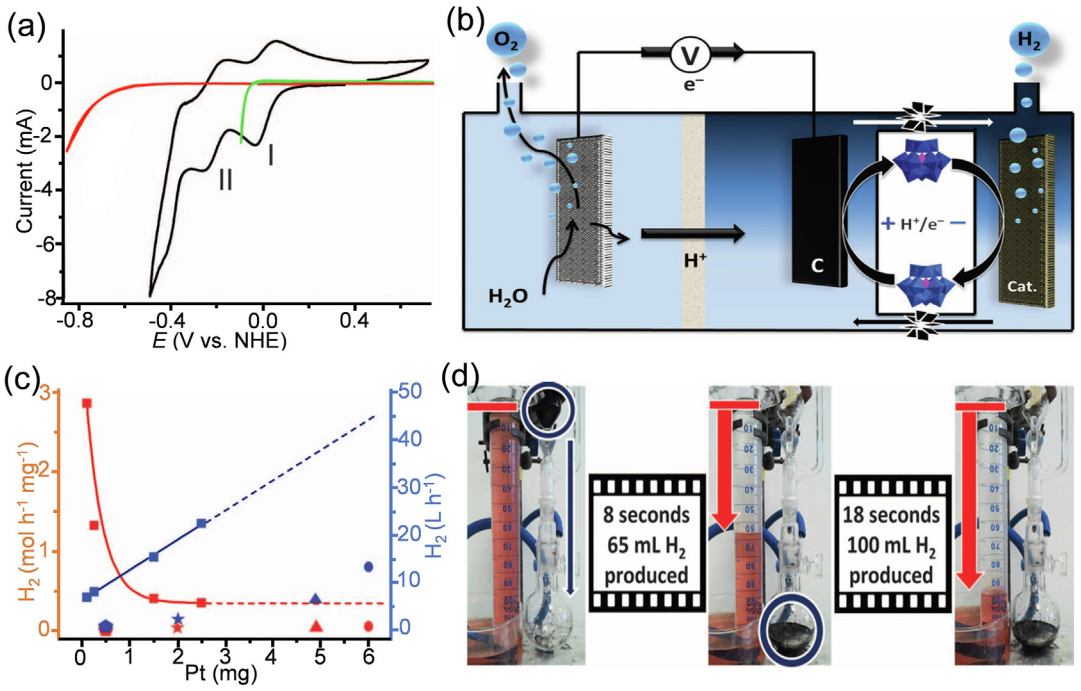


Fig. 5. (a) Reductive CVs of 0.5 M $H_4SiW_{12}O_{40}$ at pH 0.5 (black) on a GC electrode, 1.0 M H_3PO_4 at pH 1.0 on a GC (red) or Pt (green) electrode. (b) A schematic of silicotungstic acid-mediated H_2 evolution from water. (c) Comparison of the rate of H_2 production possible using electrolysis mediated by silicotungstic acid (square) and some recent state-of-the-art electrolyzers (pentagons, stars, triangles, and dots). (d) The typical apparatus configuration for determining volumes of H_2 evolved when $H_6SiW_{12}O_{40}$ was exposed to powdered catalysts. Reproduced with permission from Ref. [64]. Copyright 2013, the American Association for the Advancement of Science.

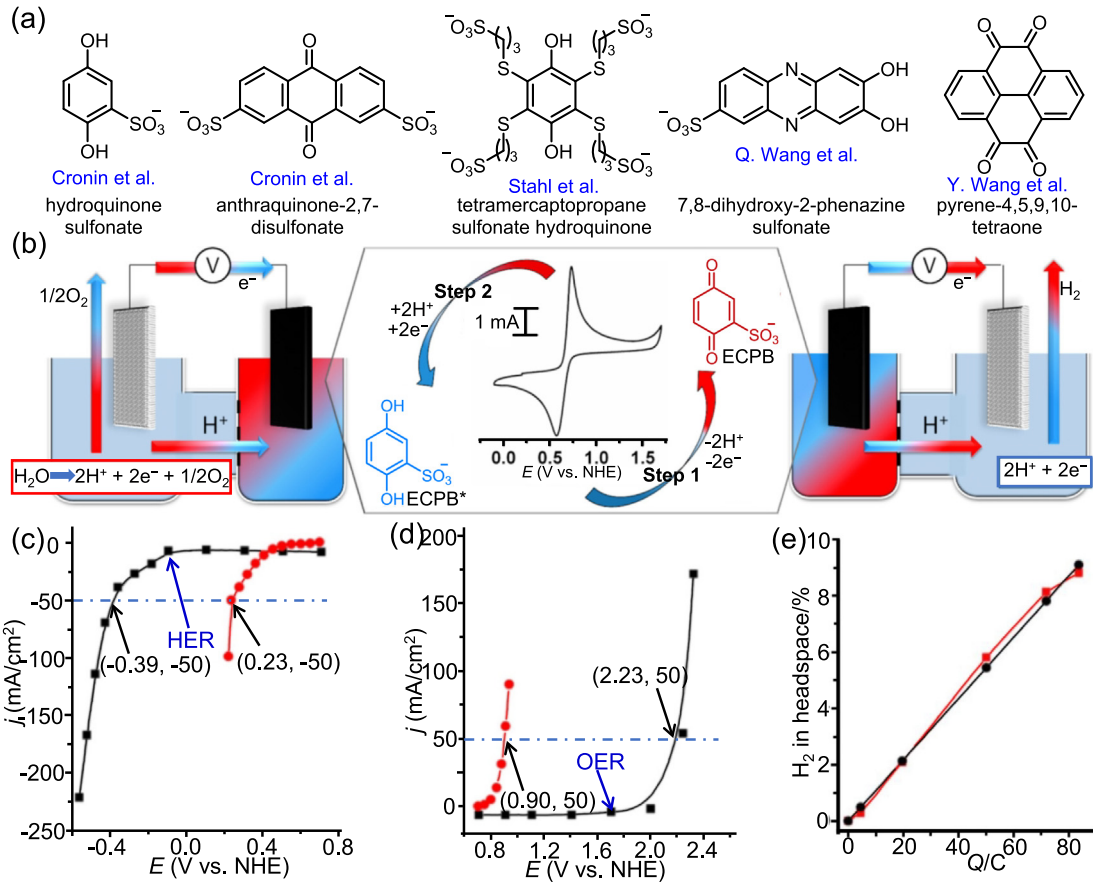


Fig. 6. (a) The reported (hydro)quinones for decoupled water electrolysis. (b) Hydroquinone sulfonate-mediated H_2O splitting with decoupled OER and HER. CV shows a 10 mM solution of the hydroquinone sulfonate in 1.8 M H_3PO_4 at pH 0.7. (c) *i-V* curves for reduction of ECPB (red) and HER (black). (d) *i-V* curves for oxidation of ECPB* (red) and OER (black). (e) A representative trace showing %H_2 expected in the cell headspace. (b–e) Reproduced with permission from Ref. [72]. Copyright 2013, American Chemical Society.

that the two-step ECPB process requires two smaller instantaneous power inputs (1.29 and 2.00 V) than the corresponding single-step reaction (2.62 V) to split water at a given current density, but the overall voltage requirement for the decoupled system (3.29 V) is higher than that for a single-step one, leading to an optimum expected efficiency of 80% for the former relative to the later. Moreover, the amount of hydrogen produced nearly corresponded to the full Faradaic efficiency (Fig. 6e, 98% ± 7%). An observable decrease in charge storage capacity of this hydroquinone sulfonate is detected during stability tests because the ability to reduce its oxidized form would decrease by approximately 1% per cycle (over 20 cycles). The oxidized form is somewhat unstable owing to self-oligomerization, which makes larger or sterically hindered quinones more intriguing. For example, the charge capacity of anthraquinone-2,7-disulfonate (Fig. 6a) shows a slight decrease of less than 0.06% per cycle (over 100 consecutive cycles); therefore, the overall capacity is substantially improved, and its redox wave maintains perfect reversibility over the same number of cycles [73]. Furthermore, a water-soluble quinone with four sterically hindered groups (i.e., mercaptopropanesulfonate, Fig. 6a) exhibits significantly enhanced stability relative to the above anthraquinone-2,7-disulfonate, and retains well its charge capacity, with a weak decay less than 1.5% after nine days [75]. In addition, a decoupled water electrolyzer using 7,8-dihydroxy-2-phenazinesulfonate as a continuous-flow RM can steadily assist hydrogen production, and the cell voltage retained at 1.53 V for more than 80 h without obvious degradation. Taken together, these quinone derivatives also show desirable stability and reversibility [76].

There are a few water-soluble (hydro)quinone derivatives, and it is laborious to introduce hydrophilic functional groups (e.g., sulfonate and phosphate) into their molecular skeletons. In 2019, Wang's group first reported that the pressing of a thin film containing pyrene-4,5,9,10-tetraone (PTO), a multicarbonyl compound that is nearly insoluble in water, onto a Ti mesh current collector, which could be utilized as an intermediate electrode to separate the HER and OER in acid [74]. Based on the enolization reaction (i.e., n-type doping reaction), solid-state PTO can theoretically store and donate four pairs of electrons and protons (Fig. 7a). The newly prepared PTO exhibits a nanorod-like morphology and grows in a compact aggregated state (Fig. 7b). It has two pairs of symmetric redox peaks (0.27 and 0.39 V) in 0.5 M H_2SO_4, which are located between the starting potentials of the HER and OER (Fig. 7c). This PTO electrode shows an acceptable stability over 200 cycles, with capacity retention of approximately 80%. A home-made cell for decoupling water splitting using PTO as a mediator is shown in Fig. 7(d), with no need for an expensive membrane, which is a characteristic of common PEMWE. The recorded cell voltages of O_2 production (step 1) and H_2 production (step 2) are 1.27 and 0.6 V, respectively, with an applied current of 50 mA (Fig. 7e). Consecutive cycling tests showed that PTO was highly stable during alternating O_2 and H_2 production. Additionally, the Faradaic efficiency of H_2 production is approximately 98.7%.

These types of mediators belong to organic oxo compounds, which are characterized by strong hydrophobicity and low solubility in water. Therefore, they need to be installed with hydrophilic functional groups or immobilized on a conductive substrate. These reports present new opportunities for extending the applications of abundant organic carbonyl compounds from rechargeable batteries to decoupled electrolysis [131].

3.3. Battery electrodes

The reversible charge/discharge process of traditional secondary battery electrodes emerges as a prospective method for buffering metal ions and electrons, which is analogous to that of a soluble redox mediator for buffering H^+/e^- pairs. Therefore, battery electrodes with appropriately positioned redox waves, abundant reserves, and good recyclability and stability can also function as solid-state ECPB to separate the two water-splitting half-reactions. Costly proton-exchange membranes can be avoided in these cases; then the corresponding membrane resistance is significantly attenuated. The classical battery electrodes can be divided into two categories: inorganic materials [27,77–109] (such as $Ni(OH)_2$ [27,77–81], $Ni/Ni(OH)_2$ [82], and $Ni(OH)_2 + WO_3$ [83]) and organic amine materials (such as polytriphenylamine [110], polyaniline [111], and diquinoxalino[2,3-a:2′,3′-c]phenazine

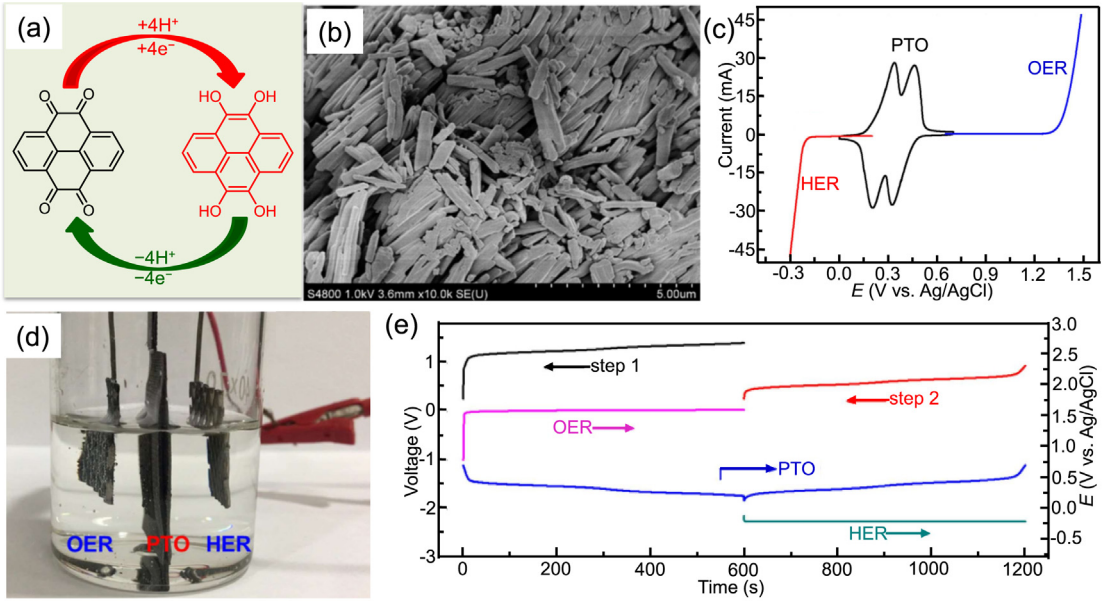


Fig. 7. (a) Schematic illustration of reaction mechanism of PTO electrode showing the function of proton and electron buffer electrode. (b) SEM image of PTO powder. (c) CV curve of the PTO electrode, LSV data of the HER and OER electrode in 0.5 M H_2SO_4. (d) Photo profiles of the decoupled water electrolysis with PTO as the redox mediator. (e) Chronopotentiometry curves of the decoupled cell at a current of 50 mA. Reproduced with permission from Ref. [74]. Copyright 2019, WILEY.

[112]). The underlying mechanism by which these heterogeneous materials store redox equivalents is associated with the reversible transformation of metal hydroxide/oxyhydroxide, ions deintercalation, and intercalation, or n-type doping/de-doping reactions (Table S1).

Polyoxometalate- and (hydro)quinone-assisted water splitting is always performed in very acidic solutions, which limit the catalysts for the OER and HER to precious metals. In 2016, Wang et al. achieved two-step water electrolysis under alkaline conditions (1.0 M KOH) using commercially available $Ni(OH)_2$/NiOOH as a robust redox mediator in a membraneless cell [77]. As depicted in Fig. 8(a), $Ni(OH)_2$ was oxidized to NiOOH, and the HER occurred simultaneously at the cathode. Subsequently, the formed NiOOH was reduced to $Ni(OH)_2$, and the OER occurred at the anode. The potential window of the $Ni(OH)_2$/NiOOH couple was exactly situated between the OER and HER onsets (Fig. 8b). Chronopotentiometry measurements at an applied current of 200 mA show that a cell voltage of nearly 1.6 V is required to drive $Ni(OH)_2$ oxidation and HER, and 0.4 V to drive NiOOH reduction and OER (Fig. 8c), implying that separate H_2/O_2 production can be flexibly completed by the output variation in fluctuating power sources (such as solar or wind power). The excellent stability and reversible transformation of this electrode are fully demonstrated by 100 uninterrupted cycles of periodic H_2/O_2 generation. Furthermore, both steps can proceed for an identical time, implying a Coulombic efficiency of 100%. Approximately 12 mL pure H_2 was collected after electrolysis at a constant current of 1.0 A for 100 s, demonstrating a high Faradaic efficiency of 94.7%. Notably, the active capacity (5 C cm^2) of $Ni(OH)_2$ did not increase, which reduced the rate of H_2 production. The achieved efficiency of the decoupled system was 92% compared to that of the alkaline water electrolyzer. Furthermore, the established two-step water electrolysis method can effectively solve the gas-mixing issue without using a membrane, and increase the utilization of fluctuating renewable energy.

In another significant report by Wang et al., decoupled acidic water electrolysis was easily realized using the organic conductive polymer polytriphenylamine (PTPAn) as the solid-state auxiliary electrode [110]. The H_2 production was accomplished via cathodic H^+ reduction and anodic n-type doping of PTPAn (oxidation of the N center in PTPAn and electrochemical adsorption of SO_4^{2-}). Subsequently, the O_2-production step was associated with anodic H_2O oxidation and n-type de-doping of $PTPAn^+$ (reduction of the N center in $PTPAn^+$ and its de-adsorption of SO_4^{2-}). The adsorption and de-adsorption of anions aims to maintain the electrical neutrality of the PTPAn organic electrode. PTPAn has an appropriately positioned potential window (Fig. 8d), indicating that it can be used as a redox mediator to decouple acidic water splitting. As shown in Fig. 8(d), the peak potential difference between the positive and negative scans is just 0.02 V, confirming the good redox reversibility of this polymer electrode. Furthermore, chronopotentiometry measurements at 5 mA applied current demonstrated that Step 1 and Step 2 required a cell voltage of 0.7 and 0.95 V, respectively (Fig. 8e). The optimized efficiency for this decoupled system was nearly 97% (1.60/1.65) relative to that of the traditional PEMWE system according to Cronin's method [50], and the former can operate at a lower input voltage and higher current than the latter (Fig. 8f). The Faraday efficiency of the H_2 production was approximately 97.8%. In addition, the Coulombic efficiency was still 100% after 120 cycles of separate H_2/O_2 generation, demonstrating that this electrode exhibits exceptional stability for decou-

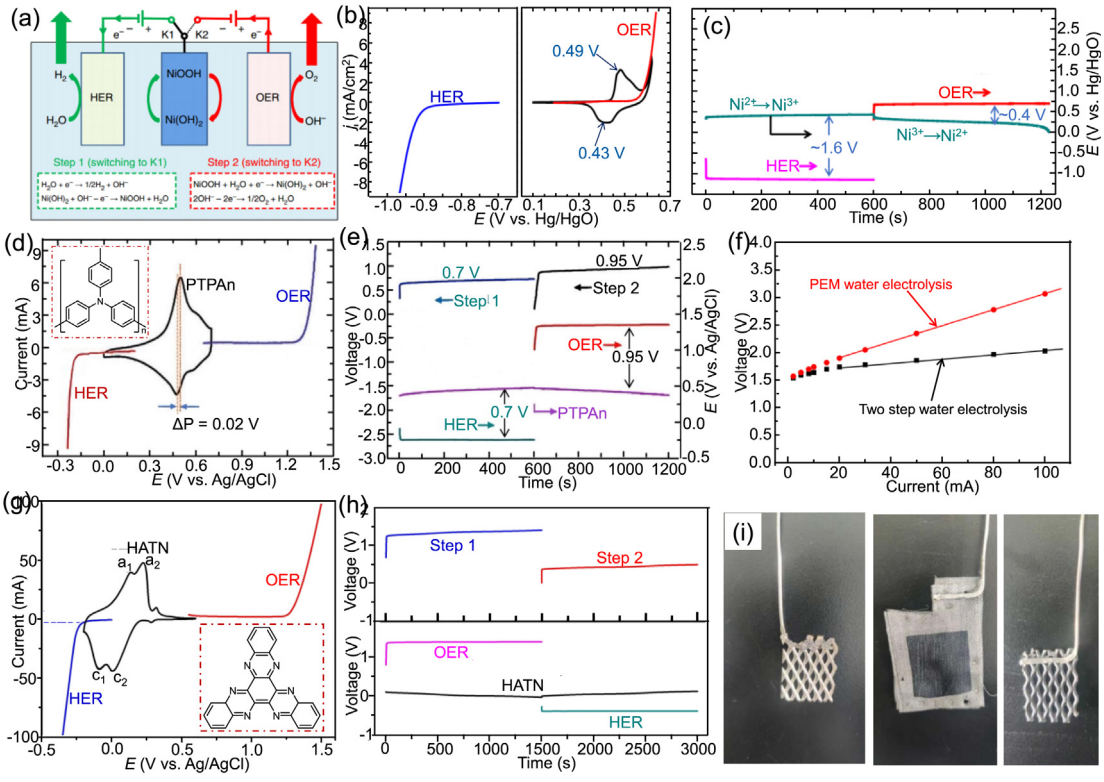


Fig. 8. (a) A schematic of the two-step water electrolysis with $Ni(OH)_2$. (b) CV curve of the $Ni(OH)_2$ (black), LSVs of RuO_2/IrO_2 electrode for the OER (red) and Pt electrode for the HER (blue). (c) Chronopotentiometry lines of the HER (pink), $Ni(OH)_2$ electrode (green), and OER (red). (a–c) Reproduced with permission from Ref. [77]. Copyright 2016, Nature. (d) CV of the PTPAn film electrode (black), LSVs of Pt for HER (blue), and RuO_2/IrO_2 for OER. Inset: The molecular structure of PTPAn. (e) Chronopotentiometry curve of the cell at 5 mA current. (f) Voltage comparison of the PEM water electrolysis and two step water electrolysis. (d–f) Reproduced with permission from Ref. [110]. Copyright 2018, WILEY. (g) CV curve of the HATN (black), the LSV of Pt-coated Ti-mesh for HER (blue) and RuO_2/IrO_2-coated Ti-mesh for OER (red) in 0.5 M H_2SO_4. Inset: The molecular structure of HATN. (h) Chronopotentiometry curve of the decoupled cell at a current of 20 mA. (i) Photograph of a Pt-coated Ti-mesh (left), HATN electrode (middle), and a RuO_2/IrO_2-coated Ti-mesh (right). (g–i) Reproduced with permission from Ref. [112]. Copyright 2023, WILEY.

pled electrolysis. Finally, membrane-free solar energy-to-hydrogen (STH) conversion was demonstrated for the first time by combining the water-electrolysis architecture with a commercial photovoltaic cell, and the STH efficiency was calculated to be 5.4%. This decoupled architecture can eliminate several challenging issues related to the use of membranes and synchronization of the OER and HER, which are widely present in common photoelectrochemical cells and photovoltaic electrolysis systems for water splitting. However, the electronic conductivity of PTPAn is not high; therefore, sufficient carbon-conductive additives are required for this film electrode.

Yang et al. recently reported that membrane-free water electrolysis can be decoupled using a phenazine-based compound (diquinoxalino [2,3-a:2′,3′-c] phenazine, HATN, Fig. 8g inset) as a solid redox mediator in an acidic solution [112]. Three pairs of reversible redox peaks were observed in the CV curve of HATN (Fig. 8g). Each pair was highly reversible and involved the acceptance/release of one proton and one electron in the C=N group, and all the peaks were located between the onset potentials for the OER and HER. The HATN electrode exhibited a high capacity retention of 51% after 3000 cycles, indicating a long cycle life. Chronopotentiometry tests showed that in the decoupled cell, the voltage inputs for O_2 production (Step 1) and H_2 production (Step 2) were nearly 1.42 and 0.5 V, respectively, under an applied current of 20 mA (Fig. 8h). The optimum efficiency of this decoupled system was approximately 92.2% (1.77/1.92) relative to that of the PEMWE system based on Cronin's method [50]. Coulombic efficiency was demonstrated to be 100%. The three electrodes used in this decoupled system are shown in Fig. 8i. Benefiting from its π-conjugated aromatic structure and fast H^+ storage/release, this imine compound exhibited high performance and outstanding durability. This compound exhibited excellent reversible stability under fluctuating current even after 500 consecutive cycles of alternating H_2/O_2 production. In particular, HATN-based decoupled devices can be driven by intermittent solar or wind energy to produce O_2 and H_2 separately. However, further technical research is needed to handle with the engineering problems of this decoupled system, including its intermittent operation, complex architecture, and poor leak-proofness.

An amphoteric water electrolysis system consisting of acidic and alkaline cells has a much lower standard potential (0.4 V) and energy consumption for splitting water than pure acidic or basic systems (1.23 V) [83,92,132]. In 2022, Šutka et al. reported that amphoteric water electrolysis was successfully decoupled using WO_3 in an acid cell (0.5 M H_2SO_4) and $Ni(OH)_2$ (1.0 M KOH) in an alkaline cell as ECPB (Fig. 9a and b), thus avoiding costly bipolar membranes [83]. According to the Nernst equation, acidic and basic solutions favor the HER and OER, respectively, making Step 2 (Fig. 9b) more favorable than Step 1 (Fig. 9a). Appealingly, O_2 and H_2 are continuously co-generated in two spatially separated cells. This novel system obviously decreases the time cost and operational complexity in comparison with the above two-step decoupled systems. Fig. 9c depicts that the redox peaks of Ni $(OH)_2$ are located more positively than those of WO_3; however, all the peaks are well-suited between the HER and OER. The chronopotentiometry curves for 10 cycles (Fig. 9d) and even 100 cycles reveal the satisfactory stability of the proposed electrolysis setup. Furthermore, the cycle time only decreased by 21% when this amphoteric electrolyzer was operated at 100 mA for 50 h, also demonstrating its gratifying stability. To obtain a current of 10 mA, the potential applied in Step 2 (0.68 V) was significantly lower than that in Step 1 (−2.93 V), and even lower than the reported amphoteric electrolysis (0.79 V) using a bipolar membrane. Moreover, the Faradaic efficiency for H_2 production in Step 1 and Step 2 is 98%.

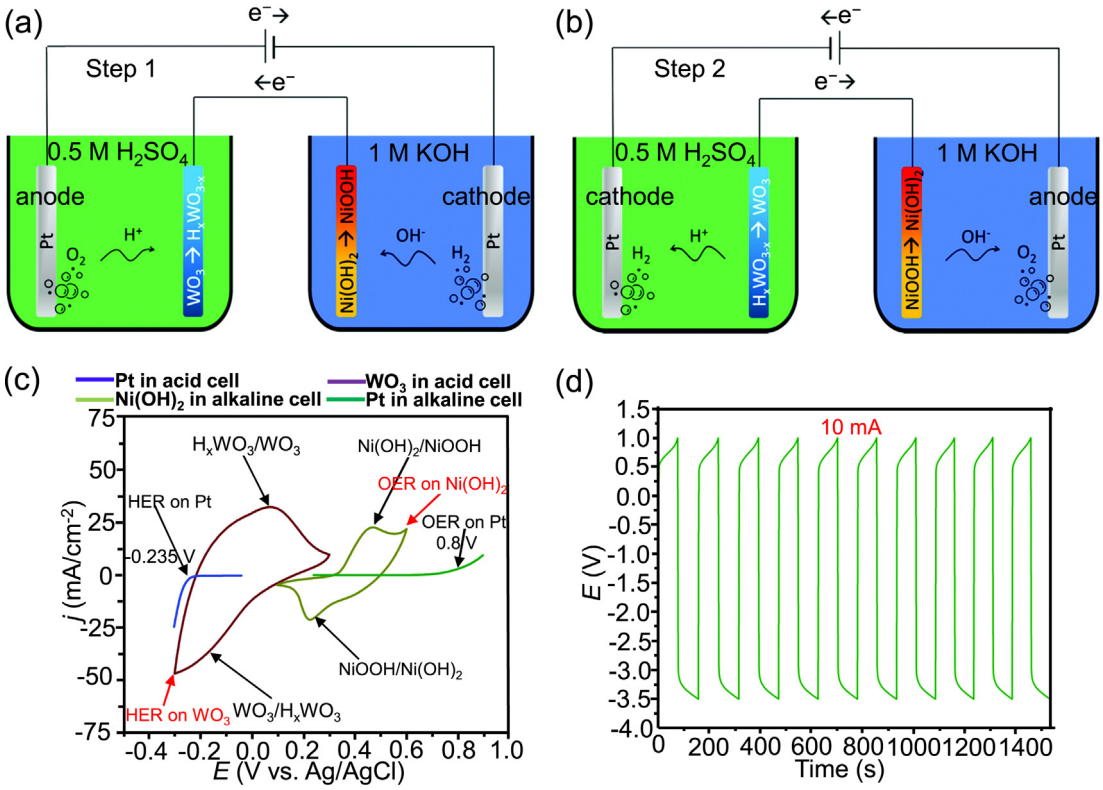


Fig. 9. (a and b) The schemes of decoupled amphoteric water electrolyser operating with opposite polarities of the applied potential. (c) Location of oxidation and reduction peaks of redox mediator electrodes between the OER and HER onset potentials. (d) Chronopotentiometry measurements for 10 cycles. Reproduced with permission from Ref. [83]. Copyright 2022, Royal Society of Chemistry.

With this amphoteric electrolysis device, H_2 and O_2 can be produced simultaneously but in different places, and obviously the combination of WO_3 and $Ni(OH)_2$ play a role similar to that of a salt bridge. The maximum total energy efficiency of the proposed amphoteric system is 71%, which is 13% higher than that of the reported alkaline decoupled electrolyzer [27] and also comparable to that of industrially available alkaline electrolyzers (70%).

3.4. Molecular metal complexes

Metal complexes are often characterized by defined structures, facile preparation, structural designability, and abundant redox activity; and they have been popularly applied in numerous fields, such as catalysis, pharmacy, energy, and environment [133–136]. Metal centers exhibit various redox states. Organic ligands can play a prominent role in modulating the redox potentials of metal centers; therefore, they are well situated between the OER and HER onset potentials, meeting the requirements for separating the OER and HER. To date, only a few complexes have been described for decoupled water electrolysis under homogeneous conditions, including ferricyanide [113–116] and (ferrocenylmethyl) trimethylammonium chloride (FcNCl) [114].

Several ECPB-type mediators (e.g., $H_3PMo_{12}O_{40}$ [50,65], $H_4SiW_{12}O_{40}$ [64,67,68], $H_6ZnW_{12}O_{40}$ [70], hydroquinone sulfonate [72], anthraquinone-2,7-disulfonate [73], and pyrene-4,5,9,10-tetraone [74]) could work only in strongly acidic solutions because their decoupling mechanisms are proton-dependent. In 2018, Sun's group reported that FcNCl, a ferrocene derivative, can function as a robust proton-independent electron reservoir to decouple water splitting in neutral solutions [114]. This iron complex (Fig. 10a inset) exhibits high water solubility exceeding 4.0 M, which is attributed to its hydrophilic structural fragment (i.e., quaternary ammonium salt). The redox couple of FcNCl is reversible and well positioned between HER and OER onsets, even with the assistance of Ni-based water-splitting electrocatalysts (Fig. 10a, NF represents nickel foam). An H-type electrolyzer for decoupled water electrolysis was constructed using FcNCl as the mediator (Fig. 10b). This device is similar to that of $H_3PMo_{12}O_{40}$ assisted water splitting reported by Cronin's group [50]. A semipermeable membrane was necessitated to avoid the diffusion of FcNCl from the counter compartment into the working one. The voltage inputs for H_2 (Fig. 10c) and O_2 (Fig. 10d) production were dramatically reduced in the presence of 50 mM FcNCl. Impressively, a high efficiency of 96% was demonstrated for this decoupled system in relation to one-step direct water splitting. A Faradaic efficiency close to 100% for H_2 evolution was obtained at a constant voltage bias. In the presence of FcNCl, alternating H_2 and O_2 production was steadily driven by electrical and solar energy (Fig. 10e and f). The remarkable cycling stability of FcNCl for repeated oxidation and reduction was demonstrated over 20 successive cycles (Fig. 10e).

In 2022, Zhang et al. rationally designed a new type of decoupled water-splitting apparatus using inexpensive ferricyanide as a proton-independent electron reservoir in 1.0 M KOH (Fig. 11a) [115]. Furthermore, the OER and HER electrodes were fabricated from earth-abundant transition metals but not from noble Pt sheets. Electrochemical tests demonstrated that the redox peaks of ferricyanide resided well between those of the OER and HER (Fig. 11b). This well-designed device also exhibited superior cyclicity for the long-term separation of H_2 and O_2 (Fig. 11c). To deliver a current density of 10 mA/cm^2, the combined voltage required by this decoupled system was 1.55 V, which was lower than that of the alkaline water electrolyzer (1.74 V). Furthermore, no obvious decay was observed over successive 15 cycles, implying the robust stability of ferricyanide in the decoupled HER from the OER.

To date, the reported molecular complexes for decoupled hydrogen production are still scarce, and they can merely buffer electrons from the OER depending on the redox-active metal center but cannot concurrently accept charge-balancing protons. Notably, one molecular complex can buffer only one electron because of the single-electron redox process at the Fe center. Predictably, the metal center of the complex should extend from Fe to other earth abundant transition metals (e.g., Cu, Co, Ni, or Mn). FcNCl and $K_4Fe(CN)_6$ are mononuclear complexes, and bi- or polynuclear complexes have been elaborately designed for decoupled H_2 production. The metal complexes with coordinated H_2O/OH^- would be likely explored as the novel type of redox mediator for decoupled water electrolysis, provided that metal center and coordinated H_2O/OH^- could buffer electrons and protons, respec-

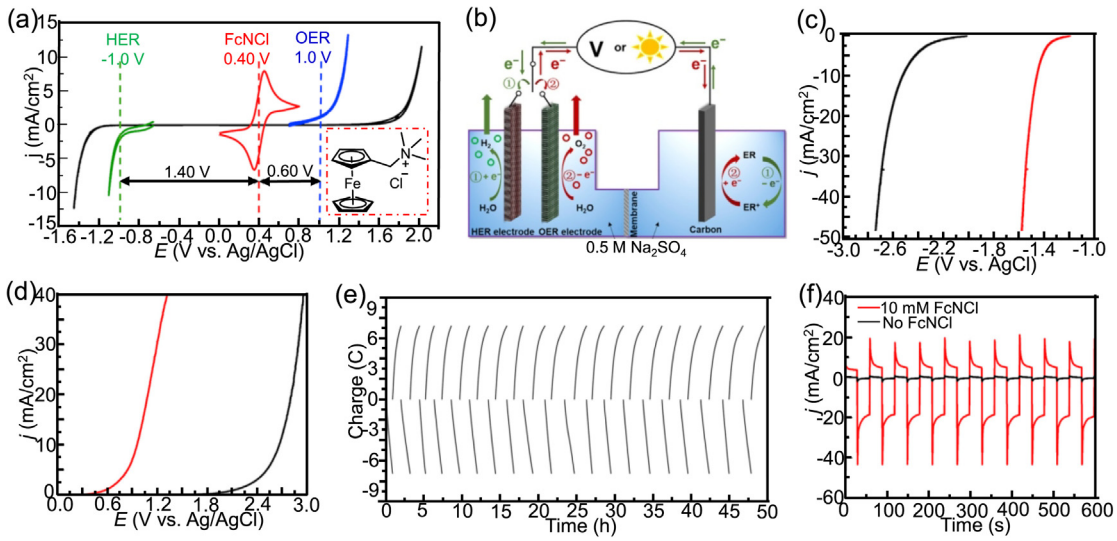


Fig. 10. (a) CVs of FcNCl (red), HER (black and green), and OER (blue and black) in 0.5 M Na_2SO_4 (pH = 6.5) with GC (red, black), Ni_2P/Ni/NF (green) or bare NF (blue) as the working electrode. Inset: The molecular structure of FcNCl. (b) An electrolyzer design for decoupled water splitting with stepwise HER and OER in near-neutral electrolyte. ER and ER$^+$ denote the reduced (i.e., FcNCl) and oxidized (i.e., FcNCl$^+$) forms of the adopted electron reservoir, respectively. LSVs of Ni_2P/Ni/NF (c) or NF (d) as the working electrode and a carbon rod as the counter electrode with 0 (black) or 50 mM (red) FcNCl and 0.5 M Na_2SO_4 in the counter chamber and only 0.5 M Na_2SO_4 in the working compartment. (e) Electrolysis cycles of HER and OER for assessing the stability of FcNCl as an electron reservoir. (f) HER current density on Ni_2P/Ni/NF produced over time under chopped sunlight irradiation with no external voltage bias. Reproduced with permission from Ref. [114]. Copyright 2018, Elsevier.

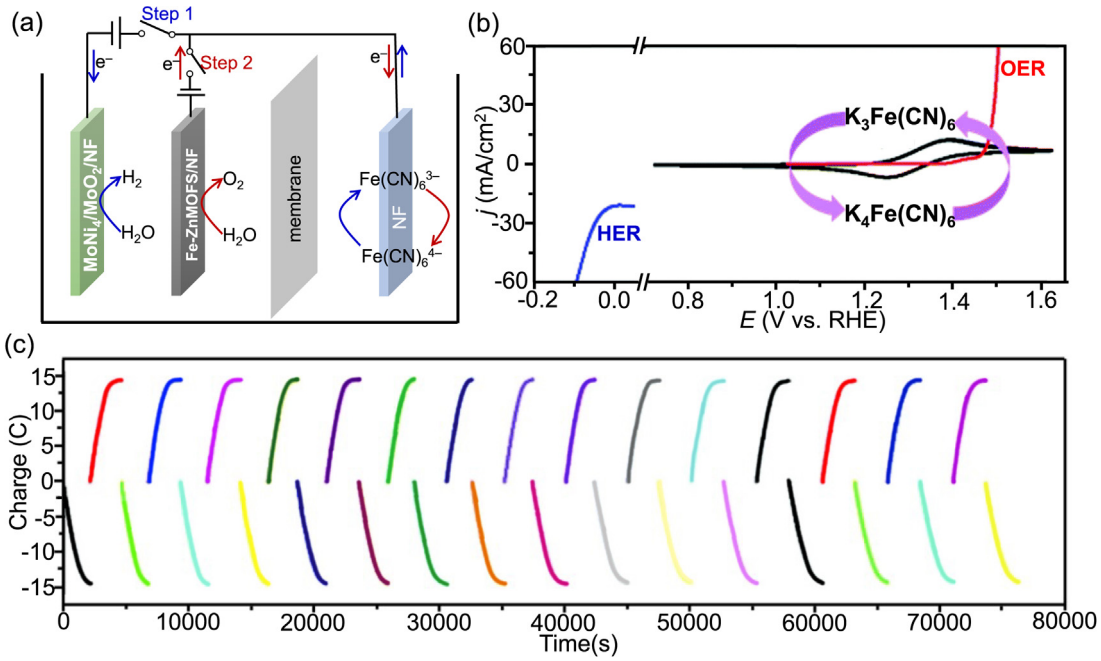


Fig. 11. (a) Schematic diagram of the decoupled water splitting system with $K_4Fe(CN)_6$ as redox mediator. (b) CV curve of the glassy carbon electrode in 1.0 M KOH and 0.3 M $K_4Fe(CN)_6$ solutions. (c) Stability measurements of decoupling water splitting. The applied voltage was alternated at 0.35 V for OER and −1.45 V for HER periodically. Reproduced with permission from Ref. [115]. Copyright 2022, Royal Society of Chemistry.

tively [137]. Furthermore, the presence of coordinated water molecules could endow the complexes with good water solubility.

3.5. Flow batteries

As seen from the above discussion, H_2 and O_2 are fundamentally generated step-by-step in decoupled water splitting using polyoxometalates, (hydro)quinones, battery- electrodes, or metal complexes as redox mediators; however, the time cost of H_2 production is doubled compared to that of traditional water splitting. Recently, H_2 and O_2 have been produced simultaneously but in different spaces via redox flow batteries based on different couples, such as $VSO_4/Ce_2(SO_4)_3$ [117], VO^{2+}/V^{3+} [118], Fe^{3+}-triethanolamine/K_2MnO_4 [119], and Ce^{4+}/Ce^{3+} [120]. This new closed-loop electrochemical-chemical cycle for indirect water splitting substantially reduce the time cost of H_2 production.

In 2014, Girault et al. reported that H_2 and O_2 could be produced concurrently in separate reactors using vanadium cerium redox flow battery (V-Ce RFB), thereby reducing the time required for H_2 production [117]. The redox potential of Ce^{4+}/Ce^{3+} was higher than that of V^{3+}/V^{2+}; however, both were between the OER and HER onset potentials (Fig. 12a). In the first circuit, the electrolytes are conventionally charged ($Ce^{3+} + V^{3+} \rightarrow Ce^{4+} + V^{2+}$). In the second one, the discharging steps of V^{2+} and Ce^{4+} were parallel to Mo_2C-catalyzed HER ($2V^{2+} + 2H^+ \rightarrow 2V^{3+} + H_2$) and RuO_2-catalyzed OER ($2Ce^{4+} + H_2O \rightarrow 2Ce^{3+} + 1/2O_2 + 2H^+$), respectively (Fig. 12b). H_2 and O_2 bubbles were clearly observed when the electrolyte flowed through the catalytic bed (Fig. 12c), and the reaction yield of H_2 gas was 96 ± 4%. Therefore, the chemical reactors that split water into O_2 and H_2 can be regarded as external loads for the V-Ce RFB module. The redox potentials of Ce^{4+}/Ce^{3+} and V^{3+}/V^{2+} were between the thermodynamic and observed potentials for the OER and HER, respectively (Fig. 12d). Hydrogen can be continuously produced using the V-Ce RFB device, and the overall energy efficiency of this system is approximately 50%.

In decoupled water electrolysis systems, the HER and OER are not closely correlated, and the HER is essentially a half-reaction of particular interest, implying that the useless OER side can be replaced. For example, OER can be replaced by the toxic SO_2 oxidation ($SO_2 + 2H_2O \rightarrow H_2SO_4 + 2H^+ + 2e^-$, Fig. 13a) [118] or MnO_4^{2-} one-electron oxidation ($MnO_4^{2-} - e^- \rightarrow MnO_4^-$, Fig. 13b) [119] for discharge of the negative electrolyte in those novel apparatus integrating RFB and HER. Under these circumstances, H_2 is the only gas produced when charged battery electrolytes (e.g., V^{2+} ions [118] and Fe^{2+}-triethanolamine [119]) are subjected to HER catalyst.

3.6. Others

Recently, polysulfides [121], hexacyanoferrate [122], V^{3+}/V^{2+} [123], VO_2^+/VO^{2+} [124], YH_x-Pd, $LaNi_{4.5}Al_{0.5}$-Pd [125], and BrO_3^-/Br^- [126] have been explored as charge mediators for HER/OER decoupling. For decoupled H_2 production assisted by the abovementioned RFBs, one tank and pump for the continuous storage and transportation of the anolyte are indispensable for forming a dual-circuit system [117–120]. In practice, dynamic circuit systems for the oxidation of water and other species can be given up, because the real focus of circuit RFBs is the steady generation of hydrogen. Decoupled water splitting has been achieved using hexacyanoferrate (Fig. 13c) [122], V^{3+}/V^{2+} (Fig. 13d) [123] or VO_2^+/VO^{2+} (Fig. 13e) [124] as the redox flow mediator for HER via a single-circuit system.

For example, Chen et al. designed a decoupled water electrolysis system consisting of a proton exchange membrane electrolysis cell for high-pressure H_2 generation (Step 1) and an H-cell for low-pressure O_2 generation (Step 2) with a VO_2^+/VO^{2+} couple as the bifunctional mediator (Fig. 13e), thus reducing the capital expenditure cost of mechanical H_2 compression [124]. Issues related to H_2-O_2 mixing were also eliminated at an increased current density. In this decoupled system, the target H_2 gas can be output at a high pressure of 35 MPa whilst avoiding hydrogen crossover, which cannot be realized via most of the commercialized PEMWE ($\leq$ 3.5 MPa). Chronopotentiometry measurements verified that at a current of 5 mA, the average cell voltages of Steps 1 and 2 were 1.24 and 0.76 V, respectively (Fig. 13f). And the corresponding

energy efficiency was evaluated as 61%, which would decrease at a higher current. It should be emphasized that Steps 1 and 2 are simultaneously performed in 1.5 M H_2SO_4, which is attributed to the pump-driven circulating flow of the V-based electrolyte. Moreover, the Faraday efficiency for H_2 production continuously declined from an estimated 92.1% to 70.5% with an increase in cathodic pressure (from 0.1 to 35 MPa). The reliable stability of this high-pressure decoupled system was verified by a cycling performance test for nearly 120 h.

Another electrolytic mode for decoupling the HER and OER during the water splitting process can be achieved with thermodynamically and economically favorable organic oxidation in place of the OER to synchronize with the HER [138–145]. However, this mode is now more suitable to be called as 'hybrid water splitting' [39–41]; therefore, a detailed description of these studies is not given here.

4. New applications for decoupled electrolysis

Decoupled electrolysis technology paves the way for producing high-purity H_2 efficiently and safely, whereas O_2 generated at the anode is always acknowledged as a useless by-product [39–41]. It has been demonstrated that the OER can be replaced by the synthesis of high value-added chemicals [114], or pollutant oxidation [118], and the discharging process of liquid fuel cells [79], NiOOH-Zn battery [146], and Zn-hydrazine battery [147]. Furthermore, hydrogen equivalents buffered in mediators can be applied for the catalytic hydrogenation of unsaturated organic compounds, completing tandem hydrogen production and in situ utilization [129,148,149]. Importantly, this decoupled concept has been extended to chlor-alkali process [147] and other half-reactions in artificial photosynthesis [150], such as CO_2 reduction [151,152].

5-Hydroxymethylfurfural (HMF) is an important biomass model compound, and its electro-upgrading has attracted substantial attention. In an important report by Sun's group, commercial $Na_4[Fe(CN)_6]$ served as the electron mediator (ER) for stepwise HER and HMF oxidation in 1.0 M NaOH (Fig. 14a) [114]. In the two-compartment H cell, a Co-P/NF, NF, and carbon rod were used as electrodes for the HER, HMF oxidation, and redox cycling of the mediator, respectively. According to electrochemical tests, both $Na_4[Fe(CN)_6]$ (Fig. 14b) and HMF (Fig. 14c) were much easier to oxidize than H_2O. The HER and HMF oxidation are promoted by this mediator. Two valuable products (H_2 and 2,5-furandicarboxylic acid) were successively generated, and O_2-related issues were obviated via decoupled electrolysis. The usefulness of the oxidative potential has been improved. Besides, a formal Faradic efficiency of 200% can be achieved. This novel mode not only reshapes hydrogen production via water splitting, but also promotes the green manufacture of chemicals.

In 2018, Wang's group reported that the familiar chlor-alkali process ($2NaCl + 2H_2O \rightarrow 2NaOH + H_2 + Cl_2$) can be decoupled into two independent steps with $Na_{0.44}MnO_2$ electrode as a redox mediator without using a membrane [146]. In the first step (Fig. 15a, left), water reduction is coupled to Na^+ de-intercalation of $Na_{0.44}MnO_2$ in 1.0 M NaOH, producing H_2 and NaOH ($H_2O + Na_{0.44}MnO_2 \rightarrow H_2 + NaOH + Na_{0.44-x}MnO_2$). Then, in the second step (Fig. 15a, right), the chlorine evolution reaction (CER) is matched with Na^+ intercalation of $Na_{0.44-x}MnO_2$ ($NaCl + Na_{0.44-x}MnO_2 \rightarrow Cl_2 + Na_{0.44}MnO_2$), generating chlorine gas in another cell containing a saturated NaCl solution. This decoupling process is similar to that in the old mercury cell, which utilizes Hg/NaHg as the redox mediator; however, the former has lower power consumption and pollution. As shown in Fig. 15(b), all the desodiation/sodiation peaks of $Na_{0.44}MnO_2$ were well positioned between the onset potentials for the CER and HER. As shown in Fig. 15(c), an average cell voltage of 1.3 V was required to achieve H_2/NaOH production (Step 1), and the average cell voltage for Cl_2 production (Step 2) was approximately 1.07 V. This fascinating decoupling strategy based on the Na^+-storage reaction has promoted the development of clean and membrane-free chlor-alkali technology.

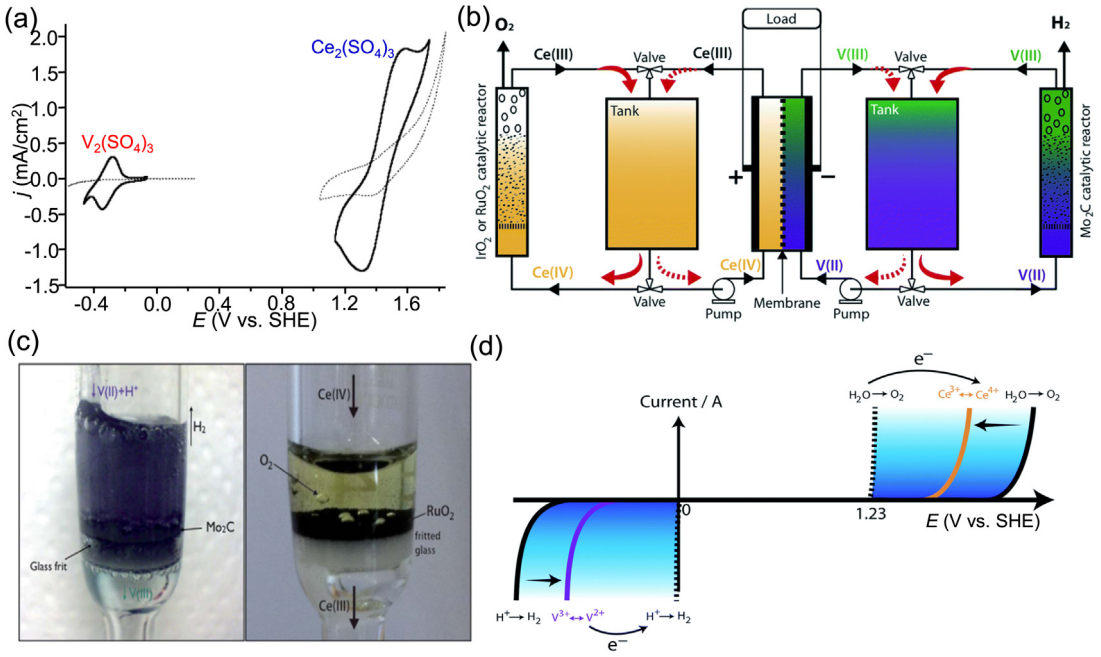


Fig. 12. (a) CVs of vanadium sulfate and cerium sulfate in 1.0 M H_2SO_4 (solid line) and 1.0 M H_2SO_4 (dashed line). (b) Schematic illustration of indirect water electrolysis as an alternative discharge process for a dual-circuit V-Ce RFB. (c) Left: HER from a V^{2+} solution on a Mo_2C catalytic bed. Right: OER from a Ce^{4+} solution on a RuO_2 catalytic bed. (d) Principle of indirect water electrolysis based on a V-Ce RFB. Reproduced with permission from Ref. [117]. Copyright 2014, Royal Society of Chemistry.

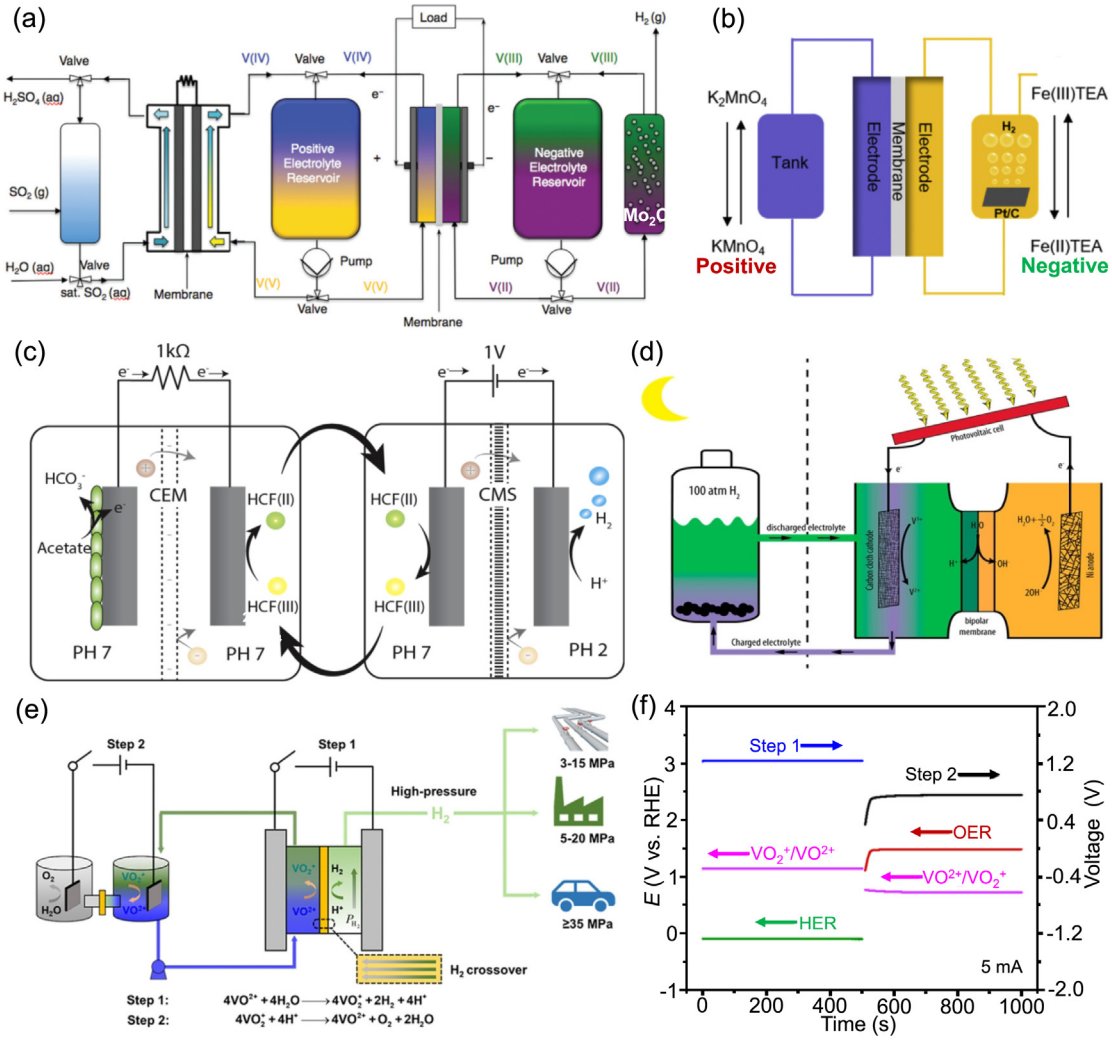


Fig. 13. (a) H_2 production via a dual-circuit redox flow battery utilizing a SO_2 fuel cell. Reproduced with permission from Ref. [118]. Copyright 2014, Royal Society of Chemistry. (b) Schematic of Fe^{3+}-TEA/K_2MnO_4 redox flow battery with hydrogen evolution in the negative tank. TEA: triethanolamine. Reproduced with permission from Ref. [119]. Copyright 2020, Elsevier. (c) Schematic view of the microbial fuel cell (left)-decoupling electrolysis system (right) apparatus. The potassium hexacyanoferrate (KHCF) (II) and (III) are noted as HCF(II) and HCF(III), respectively. Reproduced with permission from Ref. [122]. Copyright 2018, Elsevier. (d) Schematic illustration of a solar-driven V^{3+}/V^{2+} (H_2SO_4)|KOH cell. Reproduced with permission from Ref. [123]. Copyright 2019, American Chemical Society. (e) Schematic illustration of the decoupled system for high-pressure H_2 production. (f) Potential-time curves of the working and counter electrodes and cell voltage–time curves. Reproduced with permission from Ref. [124]. Copyright 2023, American Chemical Society.

5. Summary and outlook

The decoupled water electrolysis represents an emerging technology for H_2 production from water, and it indeed has numerous appealing advantages compared to the existing mature commercial PEM system. First, O_2 and H_2 can be generated at different times, rates, and even places, avoiding the formation of hazardous H_2/O_2 mixture, gas crossover, and harmful reactive oxygen species. Target H_2 can be safely produced with high purity, overcoming laborious H_2/O_2 separation and purification [50,64]. Second, low-voltage inputs are required for water splitting using the redox mediators; thus, unstable energy inputs (e.g., solar and wind) can be efficiently utilized to split water into H_2 and O_2 [65,108,110,111,114]. Third, expensive PEM can be avoided, which significantly reduces the equipment cost for H_2 production [99,110–112]. Fourth, persistent electrolysis for decoupled water splitting can be facilely achieved using redox flow barriers. In these cases, H_2 and O_2 are generated simultaneously but in different compartments, thus reducing the time cost for H_2 production [117,118]. Last but not least, high-pressure H_2 gas (35 MPa) can be efficiently produced [124]. Consequently, decoupled water splitting alleviates the series of issues resulting from the potential H_2/O_2 crossover in the conventional water splitting, but also hopefully upgrades the hydrogen storage and transportation technique.

Understanding the dependence of RMs on electrode materials is important for constructing an efficient decoupled system. Driving the redox reactions of RMs inevitably requires the assistance of electrodes. Homogenous molecular RMs (e.g., $H_3PMo_{12}O_{40}$ [50], $H_4SiW_{12}O_{40}$ [64,67,68], $H_6ZnW_{12}O_{40}$ [70], benzoquinone sulfonate [72], 9,10-anthraquinone-2,7-disulfonate [73], tetramercaptopropanesulfonate quinone [75], 7,8-dihydroxy-2-phenazinesulfonic acid [76], FcNCl [114], and $Na_4[Fe(CN)_6]$ [114]) possess high water solubility. Commercial carbon materials (e.g., carbon felt [64,67,68,72,73,76], carbon cloth [70], carbon paper [75], and carbon rod [114]) are always utilized as the RMs electrodes for sequential electrolysis; moreover, they show strong acid and alkali corrosion resistance. In contrast, metallic Pt mesh [50] and nickel foam [115] are rarely used. Heterogeneous RMs (e.g., PTO [74], Ni$(OH)_2$ [77,79,81–85], $Ni_{0.9}Co_{0.1}(OH)_2$ [80], active carbon [96,100,103], CuFe-TBA [99], FeO_x [100], Co_2P/CoP [101], Ni-Mn-P

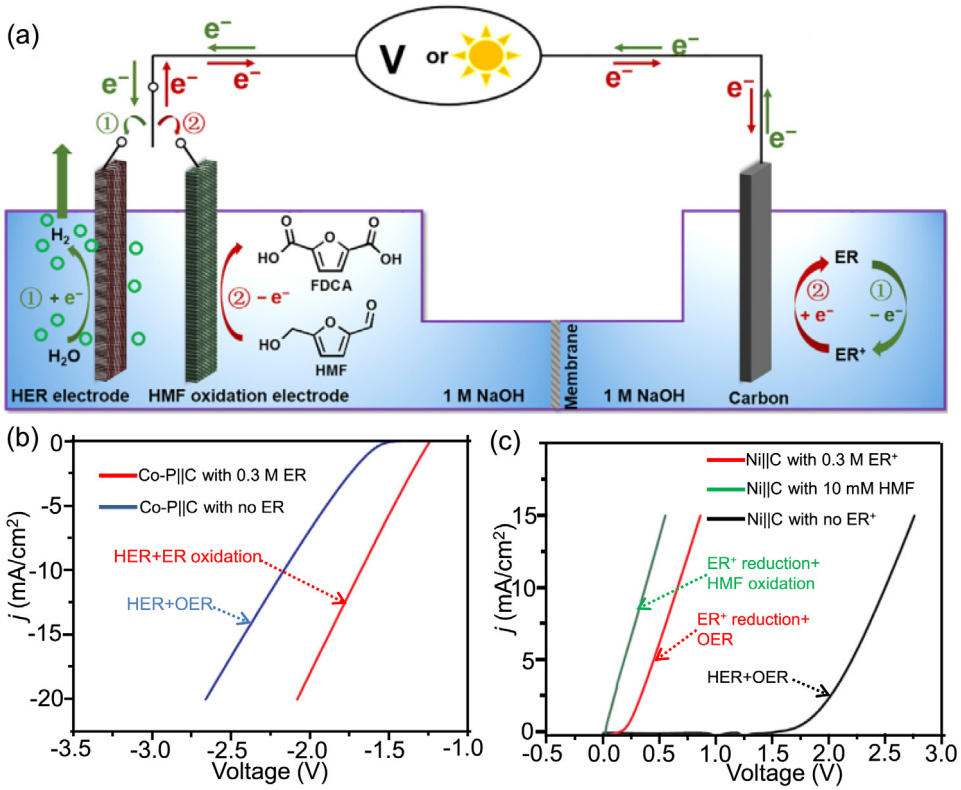


Fig. 14. (a) An electrolyzer design for stepwise HER and organic oxidation in alkaline electrolyte. (b) LSVs of the H-cell consisting of a Co-P working electrode and a carbon counter electrode with (red) or without (blue) $Na_4[Fe(CN)_6]$ (ER) in the counter compartment. (c) LSVs of the H-cell consisting of a NF working electrode and a carbon counter electrode: neither $Na_3[Fe(CN)_6]$ (ER^+) nor HMF in both compartments (black); ER^+ in the counter compartment (red); HMF in the working compartment and ER^+ in the counter compartment (green). Reproduced with permission from Ref. [114]. Copyright 2018, Elsevier.

[102], $PTPA_n$ [110], PANI [111], HATN [112], and other battery electrodes [87–98,104–108]) are easily separated from the electrolyte after sequential bulk electrolysis. The common nickel foam [80,85,87–89,91,100–102,104] and Ti-mesh [74,93,95,96,99,106,108,110–112] are frequently employed as the current collectors and substrates for loading such RMs; and nickel

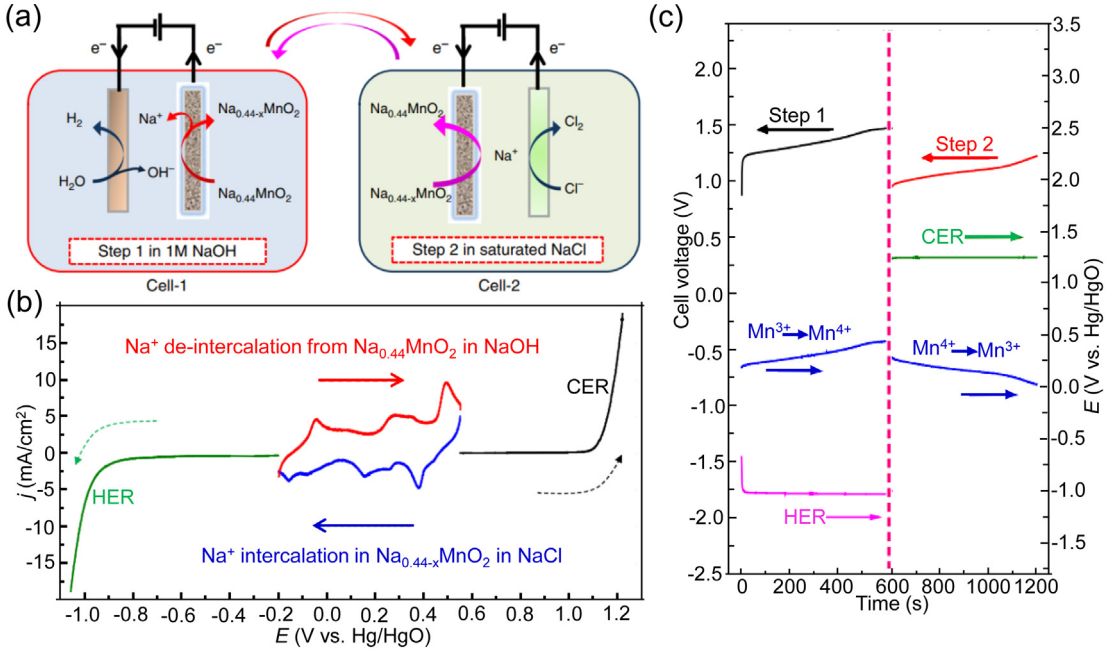


Fig. 15. (a) Schematic illustration of two-step chlor-alkali electrolysis. (b) LSVs of Na^+ de-intercalation from $Na_{0.44}MnO_2$ in 1.0 M NaOH (red) and Na^+ intercalation in $Na_{0.44-x}MnO_2$ in a saturated NaCl solution (blue); (c) chronopotentiometry curves (cell voltage vs. time) of Step 1 (NaOH + H_2 production in Cell 1) and Step 2 (Cl_2 production in Cell 2) at a constant applied current of 100 mA. Chronopotentiometry data (potential vs. time) of the HER electrode (pink line), CER electrode (green line) and $Na_{0.44}MnO_2/Na_{0.44-x}MnO_2$ electrode (blue line). Reproduced with permission from Ref. [146]. Copyright 2018, Nature.

grid [77,79], carbon materials (e.g., carbon cloth [84,98,105], carbon felt [92], graphite felt [107]), and fluorine-doped tin oxide [97] are occasionally used as electrodes. For ionic RMs (e.g., Ce^{4+}/Ce^{3+} [117] and V^{3+}/V^{2+} [117,118]), membrane electrode assemblies can easily be constructed for liquid flow batteries. The aforementioned electrodes for RMs often exhibit excellent recyclability during continuously switching between electron/proton storage and release on electrode materials, implying that such continuous switching does not adversely affect the stability of the electrode materials.

Our review aims to emphasize the chronological separation of H_2 and O_2 production via decoupled water electrolysis with the assistance of different redox mediators. This new electrolysis mode has made significant progress over the past 10 years and is strongly dependent on the design of the redox mediators. Ideal mediators should be characterized by a low molecular weight, large proton-electron capacity, good reversibility, superior stability, abundant reserves, appropriately positioned redox peaks, and even high solubility in water. Up to now, the reported RMs cannot possess all the above characteristics. The design principles of RMs should be in line with the basic principle of decoupled water splitting (Fig. 2) and possess the majority of the characteristics of an ideal RM. Moreover, diversified decoupling mechanisms have been revealed for RMs assisted water splitting (Table S1). Deep insight into the relationship between decoupling agents and decoupling mechanism is also important for further developing highly efficient H_2 production based on the decoupled strategy. Hitherto, battery electrodes account for the largest proportion of the reported RMs (Fig. 1b). Significant efforts have been deployed in the research and development of rechargeable batteries, and numerous materials have been reported as low-cost electrodes with large capacity, high stability, and long lifetime. Those electrode materials are expected to be exploited as the high-performance RMs for decoupling water electrolysis. Therefore, the development of decoupled water splitting is promisingly driven by the progress of secondary battery technology. According to the following discussion, the reported mediators always possess some of the aforementioned features. Therefore, flexibility in the design of mediators provides significant space for advancing this emerging technology.

(1) Polyoxometalates are actually the pioneering mediators for opening up the door of decoupled water splitting, and their decoupling mechanism is related to the electron-coupled proton transfer. They must dissolve in aqueous solutions, especially in strongly acidic media to maintain their protonation state. Photocatalytic water splitting can be decoupled using these mediators, but the feasibility for solar-to-H_2 is questionable owing to the dark color of their solutions. Their molecular weights are large, but the capacities for H^+/e^- are very low. Furthermore, the yield of hydrogen gas is unsatisfactory, because its redox potential of them is close to the theoretical value for protons reduction. In addition, polyoxometalate based mediators are still rare. Polyoxometalates with a light solution color and high storage capacities for H^+/e^- are desirable for decoupled electrolysis.

(2) (Hydro)quinone derivatives are developed into the decoupling agents based on bionics. These mediators can dissolve in water with the help of hydrophilic groups, such as sulfonate, or they can be supported on a conductive substrate. They can even participate in forming a flow dual electrolyzer to facilitate stepwise H_2/O_2 production. These mediators have small molecular weights and well-defined structures and they can accept and donate H^+/e^- couples via keto-enol tautomerism; therefore, a strongly acidic electrolyte is also essential.

(3) Battery-electrodes can divide water splitting into two steps mostly through the ion insertion/extraction mechanism, which is similar to the reversible charging and discharging processes in secondary batteries. Such mediators were originally applied in rechargeable batteries and supercapacitors, so electricity storage devices and hydrogen energy preparation are effectively connected. Currently, there are a large number of such mediators, and they can function in acidic or basic electrolytes, and even achieve decoupled amphoteric water splitting. Although batch operation is required to regenerate the auxiliary electrodes, these materials will be studied for use in decoupled water splitting in the future.

(4) Metal complexes can act as robust electron mediators for decoupled water splitting by relying on the gain and loss of electrons in the metal centers. The reported complexes can buffer electrons originating from the OER but not protons. They are characterized by well-defined structures, low molecular weights, enhanced designability, and high solubility in aqueous solutions. Such mediators should work in basic and neutral solutions, but they can decompose into metal ions and ligands in acidic solutions because of the decomplexation between the metal centers and ligands. To date, the reported complexes are very rare, and they belong to monuclear complexes. It is anticipated that molecular complexes that have multiple metal centers and can buffer electrons and protons would be elaborately designed for decoupled water splitting. Hopefully, the 3D electrodes for decoupled water splitting would be prepared from molecular metal complexes via immobilizing them on conductive substrate. This heterogenization process is conducive to the separation and recovery of soluble metal complexes.

(5) Liquid flow batteries can uninterruptedly produce gaseous H_2 and O_2 simultaneously but in different places, thus decreasing the time cost for hydrogen production. At least one pump is required to deliver and circulate the electrolyte. The number of known redox species (e.g., Ce and V) for constructing liquid flow batteries is very limited, hindering the application of these batteries in decoupled water splitting.

Conventional water electrolysis (including PEM and alkaline water electrolyzer) is a more mature technology than the decoupled one, thus valuable experience and lessons obtained from the scaling-up of the former can offer us beneficial inspiration for further developing the latter. To achieve widespread application of decoupled H_2 production, the size of integrated electrodes or the volume of bulk solutions made from robust RMs should be scaled up to some extent. The electrodes for the OER and HER should also be enlarged proportionally to maintain the consistency and uniformity of the redox reactions during the scaling-up process. Among the reported RMs, battery electrodes are the most common (Fig. 1b). These as-prepared RMs are solid-state powder in appearance, and are often made into thin films with the assistance of a binder and a conductive additive. The film is then pressed onto a suitable current collector to form a 3D integrated electrode. The homogeneity, interfacial conductivity, and cohesion between the RMs film and the current collector should be enhanced to prepare a large and durable intermediate electrode. The concept of roll-to-roll cable-car electrodes proposed by Wu's group has been demonstrated for uninterrupted and massive hydrogen production using common $Ni(OH)_2$ as the RM [85]. Therefore, exploring innovative modular designs is highly valuable for the scaling-up of decoupled water splitting. Liquid RMs (e.g., polyoxometalates, (hydro)quinones, and metal complexes) are highly soluble in aqueous solutions. Given the high capacity requirement for producing large volumes of H_2, such molecular RMs are promising candidates for

large-scale decoupled electrolysis via constructing redox flow batteries. This dynamic decoupled system shows high recyclability and practicability, and could reduce the usage of RMs and occupied areas of the electrolytic device. Special designs may be adopted to enhance the gas tightness and corrosion resistance.

There is still large room for improvement in the decoupled H_2 production from water. The energy-conversion efficiency of decoupled devices should be further enhanced via the rational design of stable RMs with high specific capacities. Numerous inorganic and organic electrode materials have been designed and prepared for rechargeable batteries, and an increasing number of these materials have been applied as robust RMs for decoupling water splitting. The relationship between material structure and activity should be intensively studied to develop next-generation high-performance RMs for energy-saving water splitting. Furthermore, large-sized electrodes that integrate RM with a current collector are more popular owing to their facile preparation and easy separation from electrolytes. Given that the OER product has low economic value, a combination of decoupled strategies with other oxidative reactions should be explored to co-produce pure H_2 and valuable chemicals. The development of decoupled water splitting may be accelerated using mature redox flow batteries with soluble species as RMs. Moreover, plausible strategies for scaling up should be explored to promote decoupled H_2 production at ampere-level current density. Therefore, a decoupled device with a long lifetime should be constructed. The decoupled hydrogen production would be desirably performed in seawater and even wastewater due to the extreme shortage of freshwater. More soluble redox mediators that can store and release oxygen instead of hydrogen equivalent should be exploited to build up a membraneless system for continuous operation.

Declaration of competing interest

The authors declare that they have no known competing financial interests or personal relationships that could have appeared to influence the work reported in this paper.

Acknowledgments

We gratefully acknowledge the financial support from the National Natural Science Foundation of China (52002146).

Appendix A. Supplementary material

Supplementary material to this article can be found online at https://doi.org/10.1016/j.jechem.2024.03.001.

References

[1] J. Chow, R.J. Kopp, P.R. Portney, Science 302 (2003) 1528.
[2] J. Tollefson, Nature 473 (2011) 134–135.
[3] J. Tollefson, Nature 556 (2018) 422–425.
[4] Y. Shi, M. Li, Y. Yu, B. Zhang, Energy Environ. Sci. 13 (2020) 4564–4582.
[5] N.S. Lewis, D.G. Nocera, Proc. Natl. Acad. Sci. U.S.A. 103 (2006) 15729–15735.
[6] M.S. Dresselhaus, I.L. Thomas, Nature 414 (2001) 332–337.
[7] N. Armaroli, V. Balzani, Angew. Chem. Int. Ed. 46 (2007) 52–66.
[8] A. Bernstein, E.H. Sargent, A. Aspuru-Guzik, R. Cogdell, G.R. Fleming, R. Grondelle, M. Molina, Nature 538 (2016) 30.
[9] A. Orlov, J. Sillmann, I. Vigo, Nat. Energy 5 (2020) 108–110.
[10] J.M. Thomas, P.P. Edwards, P.J. Dobson, G.P. Owen, J. Energy Chem. 51 (2020) 405–415.
[11] N. Armaroli, V. Balzani, ChemSusChem 4 (2011) 21–36.
[12] J.A. Turner, Science 305 (2004) 972–974.
[13] X. Fu, R. Shi, S. Jiao, M. Li, Q. Li, J. Energy Chem. 70 (2022) 129–153.
[14] L. Ji, C. Lv, Z. Chen, Z. Huang, C. Zhang, Adv. Mater. 30 (2018) 1705653.
[15] X. Li, L. Zhao, J. Yu, X. Liu, X. Zhang, H. Liu, W. Zhou, Nano-Micro Lett. 12 (2020) 131.
[16] J. Zhu, L. Hu, P. Zhao, L. Lee, K.-Y. Wong, Chem. Rev. 120 (2020) 851–918.
[17] M. Chatenet, B.G. Pollet, D.R. Dekel, F. Dionigi, J. Deseure, P. Millet, R.D. Braatz, M.Z. Bazant, M. Eikerling, I. Staffell, P. Balcombe, Y. Shao-Horn, H. Schäfer, Chem. Soc. Rev. 51 (2022) 4583–4762.
[18] M. Khan, H. Zhao, W. Zou, Z. Chen, W. Cao, J. Fang, J. Xu, L. Zhang, J. Zhang, Electrochem. Energy Rev. 1 (2018) 483–530.
[19] S. Tee, K. Win, W. Teo, L.-D. Koh, S. Liu, C. Teng, M.-Y. Han, Adv. Sci. 4 (2017) 1600337.
[20] W.-P. Schill, Joule 4 (2020) 2047–2064.
[21] D. Elliott, Nat. Energy 1 (2016) 15003.
[22] S.M. Barnett, K.I. Goldberg, J.M. Mayer, Nat. Chem. 4 (2012) 498–502.
[23] G. Li, G. Han, L. Wang, X. Cui, N.K. Moehring, P.R. Kidambi, D.-E. Jiang, Y. Sun, Nat. Commun. 14 (2023) 525.
[24] Z. Xiao, C. Lu, J. Wang, Y. Qian, B. Wang, Q. Zhang, A. Tang, H. Yang, Adv. Funct. Mater. 33 (2023) 2212183.
[25] J. Li, Y. Ma, C. Zhang, C. Zhang, H. Ma, Z. Guo, N. Liu, M. Xu, H. Ma, J. Qiu, Nat. Commun. 14 (2023) 8146.
[26] A. Rodríguez-Gómez, F. Dorado, P. Sánchez, A.R. Osa, J. Energy Chem. 70 (2022) 394–406.
[27] A. Landman, H. Dotan, G.E. Shter, M. Wullenkord, A. Houaijia, A. Maljusch, G.S. Grader, A. Rothschild, Nat. Mater. 16 (2017) 646–651.
[28] H. Kojima, K. Nagasawa, N. Todoroki, Y. Ito, T. Matsui, R. Nakajima, Int. J. Hydrogen Energy 48 (2023) 4572–4593.
[29] L. Ghassemzadeh, K. Kreuer, J. Maier, K. Müller, J. Phys. Chem. C 114 (2010) 14635–14645.
[30] V. Prabhakaran, C.G. Arges, V. Ramani, Proc. Natl. Acad. Sci. U.S.A. 109 (2012) 1029–1034.
[31] M. Schalenbach, M. Carmo, D.L. Fritz, J. Mergel, D. Stolten, Int. J. Hydrogen Energy 38 (2013) 14921–14933.
[32] M. Carmo, D.L. Fritz, J. Mergel, D. Stolten, Int. J. Hydrogen Energy 38 (2013) 4901–4934.
[33] C. Deng, C. Toe, X. Li, J. Tan, H. Yang, Q. Hu, C. He, Adv. Energy Mater. 12 (2022) 220104.
[34] X.-W. Lv, W.-W. Tian, Z.-Y. Yuan, Electrochem. Energy Rev. 6 (2023) 23.
[35] J. Yao, W. Huang, W. Fang, M. Kuang, N. Jia, H. Ren, D. Liu, C. Lv, C. Liu, J. Xu, Q. Yan, Small Methods 4 (2020) 2000494.
[36] Y. Wang, Y. Shang, Z. Cao, K. Zeng, Y. Xie, J. Li, Y. Yao, W. Gan, Chem. Eng. J. 439 (2022) 135722.
[37] Y. Yang, H. Zhang, Z.-H. Lin, Y. Liu, J. Chen, Z. Lin, Y. Zhou, C. Wong, Z. Wang, Energy Environ. Sci. 6 (2013) 2429–2434.
[38] P. Liu, D. Gao, W. Xiao, L. Ma, K. Sun, P. Xi, D. Xue, J. Wang, Adv. Funct. Mater. 28 (2018) 1706928.
[39] B. You, Y. Sun, Acc. Chem. Res. 51 (2018) 1571–1580.
[40] J. Du, D. Xiang, K. Zhou, L. Wang, J. Yu, H. Xia, L. Zhao, H. Liu, W. Zhou, Nano Energy 104 (2022) 107875.
[41] H.-Y. Wang, M.-L. Sun, J.-T. Ren, Z.-Y. Yuan, Adv. Energy Mater. 13 (2023) 2203568.
[42] E.M. Nichols, J.J. Gallagher, C. Liu, Y. Su, J. Resasco, Y. Yu, Y. Sun, P. Yang, M. Chang, C.J. Chang, Proc. Natl. Acad. Sci. U.S.A. 112 (2015) 11461–11466.
[43] C. Liu, B.C. Colón, M. Ziesack, P.A. Silver, D.G. Nocera, Science 352 (2016) 1210–1213.
[44] C. Liu, K.K. Sakimoto, B.C. Colón, P.A. Silver, D.G. Nocera, Proc. Natl. Acad. Sci. U.S.A. 114 (2017) 56450–56455.
[45] W. Zhang, M. Liu, X. Gu, Y. Shi, Z. Deng, N. Cai, Chem. Rev. 123 (2023) 7119–7192.
[46] W. Li, H. Tian, L. Ma, Y. Wang, X. Liu, X. Gao, Mater. Adv. 3 (2022) 5598–5644.
[47] O.F. Aldosari, I. Hussain, Z. Malaibari, J. Energy Chem. 80 (2023) 658–688.
[48] K. Zhang, M. Xu, J. Wang, Z. Chen, Nanoscale 15 (2023) 17525–17533.
[49] B. Zhou, Y. Zhang, T. Wang, W. Zhou, J. Liu, Y. Zou, L. Tao, Y. Lu, S. Wang, Chem Catal. 1 (2021) 1493–1504.
[50] M.D. Symes, L. Cronin, Nat. Chem. 5 (2013) 403–409.
[51] A.G. Wallac, M.D. Symes, Joule 2 (2018) 1390–1395.
[52] P.J. McHugh, A.D. Stergiou, M.D. Symes, Adv. Energy Mater. 10 (2020) 2002453.
[53] J. Huang, Y. Wang, Cell Rep. Phys. Sci. 1 (2020) 100138.
[54] F. Zhang, Q. Wang, ACS Mater. Lett. 3 (2021) 641–651.
[55] Z.P. Ifkovits, J.M. Evans, M.C. Meier, K.M. Papadantonakis, N.S. Lewis, Energy Environ. Sci. 14 (2021) 4740–4759.
[56] D. Yan, C. Mebrahtu, S. Wang, R. Palkovits, Angew. Chem. Int. Ed. 62 (2023) e202214333.
[57] Y. Ma, K. Wu, T. Long, J. Yang, Adv. Energy Mater. 13 (2023) 2203455.
[58] J. Du, Z. Chen, S. Ye, B.J. Wiley, T.J. Meyer, Angew. Chem. Int. Ed. 54 (2015) 2073–2078.
[59] M. Suga, F. Akita, K. Yamashita, Y. Nakajima, G. Ueno, H. Li, T. Yamane, K. Hirata, Y. Umena, S. Yonekura, L.-J. Yu, H. Murakami, T. Nomura, T. Kimura, M. Kubo, S. Baba, T. Kumasaka, K. Tono, M. Yabashi, H. Isobe, K. Yamaguchi, M. Yamamoto, H. Ago, J.-R. Shen, Science 366 (2019) 334–338.
[60] C. Zhang, C. Chen, H. Dong, J.-R. Shen, H. Dau, J. Zhao, Science 348 (2015) 690–693.
[61] W. Lubitz, E.J. Reijerse, J. Messinger, Energy Environ. Sci. 1 (2008) 15–31.
[62] R.K. Yadav, J.-O. Baeg, G. Oh, N.-J. Park, K.-J. Kong, J. Kim, D. Hwang, S.K. Biswas, J. Am. Chem. Soc. 134 (2012) 11455–11461.
[63] S.Y. Reece, J.A. Hamel, K. Sung, T.D. Jarvi, A.J. Esswein, J.J.H. Pijpers, D.G. Nocera, Science 334 (2011) 645–648.
[64] B. Rausch, M.D. Symes, G. Chisholm, L. Cronin, Science 345 (2014) 1326–1330.
[65] L.G. Bloor, R. Solarska, K. Bienkowski, P.J. Kulesza, J. Augustynski, M.D. Symes, L. Cronin, J. Am. Chem. Soc. 138 (2016) 6707–6710.

[66] F. Li, F. Yu, J. Du, Y. Wang, Y. Zhu, X. Li, L. Sun, Chem. Asian J. 12 (2017) 2666–2669.
[67] L. MacDonald, J.C. McGlynn, N. Irvine, I. Alshibane, L.G. Bloor, B. Rausch, J.S.J. Hargreaves, L. Cronin, Sustain. Energy Fuels 1 (2017) 1782–1787.
[68] W. Wu, X.-Y. Wu, S.-S. Wang, C.-Z. Lu, RSC Adv. 8 (2018) 39291–39295.
[69] J.-J. Chen, M.D. Symes, L. Cronin, Nat. Chem. 10 (2018) 1042–1047.
[70] J. Lei, J.-J. Yang, T. Liu, R.-M. Yuan, D.-R. Deng, M.-S. Zheng, J.-J. Chen, L. Cronin, Q.-F. Dong, Chem. Eur. J. 25 (2019) 11432–11436.
[71] G. Chisholm, L. Cronin, M.D. Symes, Electrochim. Acta 331 (2020) 135255.
[72] B. Rausch, M.D. Symes, L. Cronin, J. Am. Chem. Soc. 135 (2013) 13656–13659.
[73] N. Kirkaldy, G. Chisholm, J.-J. Chen, L. Cronin, Chem. Sci. 9 (2018) 1621–1626.
[74] Y. Wang, Y. Ma, Z. Guo, X. Dong, Y. Xia, Angew. Chem. Int. Ed. 58 (2019) 4622–4626.
[75] F. Wang, H. Sheng, W. Li, J.B. Gerken, S. Jin, S.S. Stahl, ACS Energy Lett. 6 (2021) 1533–1539.
[76] F. Zhang, H. Zhang, M. Salla, N. Qin, M. Gao, Y. Ji, S. Huang, S. Wu, R. Zhang, Z. Lu, Q. Wang, J. Am. Chem. Soc. 143 (2021) 223–231.
[77] L. Chen, X. Dong, Y. Wang, Y. Xia, Nat. Commun. 7 (2016) 11741.
[78] M.D. Symes, Nat. Energy 4 (2019) 730–731.
[79] Y. Ma, X. Dong, R. Wang, D. Bin, Y. Wang, Y. Xia, Energy Storage Mater. 11 (2018) 260–266.
[80] H. Dotan, A. Landman, S.W. Sheehan, K.D. Malviya, G.E. Shter, D.A. Grave, Z. Arzi, N. Yehudai, M. Halabi, N. Gal, N. Hadari, C. Cohen, A. Rothschild, G.S. Grader, Nat. Energy 4 (2019) 786–795.
[81] A. Landman, R. Halabi, P. Dias, H. Dotan, A. Mehlmann, G.E. Shter, M. Halabi, O. Naseraldeen, A. Mendes, G.S. Grader, A. Rothschild, Joule 4 (2020) 448–471.
[82] A. Landman, S. Hadash, G.E. Shter, A. Ben-Azaria, H. Dotan, A. Rothschild, G.S. Grader, Adv. Funct. Mater. 31 (2021) 2008118.
[83] M. Vanags, G. Kulikovskis, J. Kostjukovs, L. Jekabsons, A. Sarakovskis, K. Smits, L. Bikse, A. Šutka, Energy Environ. Sci. 15 (2022) 2021–2028.
[84] N. Hayek, A. Landman, Y. Halpern, I. Slobodkin, E.S. Davydova, A. Rothschild, J. Mater. Chem. A 10 (2022) 726–739.
[85] Y. Long, C. Yang, Y. Wu, B. Deng, Z. Li, N. Hussain, K. Wang, R. Wang, X. He, P. Du, Z. Guo, J. Lang, K. Huang, H. Wu, Adv. Sci. 10 (2023) 2301872.
[86] M.-J. Zhao, Q. He, T. Xiang, H.-Q. Ya, H. Luo, S. Wan, J. Ding, J.-B. He, Renew. Energy 203 (2023) 583–591.
[87] Z. Nie, L. Zhang, Z. Du, J. Hu, X. Huang, C. Zhou, T. Wågberg, G. Hu, J. Colloid Interface Sci. 642 (2023) 714–723.
[88] C. Sun, Y. He, N.S. Alharbi, S. Yang, C. Chen, J. Colloid Interface Sci. 642 (2023) 13–22.
[89] Z. Ke, L. Zhang, Q. Liu, Q. Zhu, C. Liu, G. Hu, Int. J. Hydrogen Energy 49 (2024) 862–874.
[90] W. Shao, S. Chen, B. Lu, J. Zhang, Y. Cheng, C. Zhang, F. Zhang, Chem. Eng. J. 480 (2024) 148126.
[91] B. Choi, D. Panthi, M. Nakoji, T. Kabutomori, K. Tsutsumi, A. Tsutsumi, Chem. Eng. Sci. 157 (2017) 200–208.
[92] J. Huang, Y. Xie, L. Yan, B. Wang, T. Kong, X. Dong, Y. Wang, Y. Xia, Energy Environ. Sci. 14 (2021) 883–889.
[93] X. Zheng, F. Lv, X. Liu, Z. Zheng, Y. Chen, Chem. Commun. 59 (2023) 2138–2141.
[94] M. Guo, L. Wang, J. Zhan, X. Jiao, D. Chen, T. Wang, J. Mater. Chem. A 8 (2020) 16609–16615.
[95] T. Wu, Y. Hu, M. Li, B. Han, Z. Liang, D. Geng, Int. J. Hydrogen Energy 48 (2023) 35552–35560.
[96] M. Guo, J. Zhan, Z. Wang, X. Wang, Z. Dai, T. Wang, Chin. Chem. Lett. 34 (2023) 107709.
[97] M. Vanags, M. Iesalnieks, L. Jēkabsons, A. Zukuls, A. Šutka, Int. J. Hydrogen Energy 48 (2023) 20551–20561.
[98] Z. Ma, X. Lu, S. Park, T. Shinagawa, M. Okubo, K. Takanabe, A. Yamada, Adv. Funct. Mater. 33 (2023) 2214466.
[99] S. Liang, M. Jiang, H. Luo, Y. Ma, J. Yang, Adv. Energy Mater. 11 (2021) 2102057.
[100] Z. Jin, P. Li, D. Xiao, ChemSusChem 10 (2017) 483–488.
[101] K. Zhang, G. Zhang, Q. Ji, J. Qu, H. Liu, Nano-Micro Lett. 12 (2020) 154.
[102] Z. Liu, G. Zhang, K. Zhang, H. Lan, H. Liu, J. Qu, J. Mater. Chem. A 8 (2020) 4073–4082.
[103] Y. Chen, G.Z. Chen, ACS Appl. Energy Mater. 6 (2023) 6104–6110.
[104] M. Xiang, T. Zhang, F. Tan, S. Cai, Z. Xu, Catal. Commun. 179 (2023) 106698.
[105] Y. He, C. Sun, N.S. Alharbi, S. Yang, C. Chen, J. Colloid Interface Sci. 650 (2023) 151–160.
[106] F. Wang, W. Li, R. Wang, T. Guo, H. Sheng, H.-C. Fu, S.S. Stahl, S. Jin, Joule 5 (2021) 149–165.
[107] S. Liang, Y. Ma, H. Luo, K. Wu, J. Chen, J. Yang, Chem. Eur. J. 29 (2023) e202302160.
[108] F. Lv, Z. Qin, J. Wu, L. Pan, L. Liu, Y. Chen, Y. Zhao, ChemSusChem 16 (2023) e202201689.
[109] Z. Zhu, T. Jiang, J. Sun, Z. Liu, Z. Xie, S. Liu, Y. Meng, Q. Peng, W. Wang, K. Zhang, H. Liu, Y. Yuan, K. Li, W. Chen, JACS Au 3 (2023) 488–497.
[110] Y. Ma, X. Dong, Y. Wang, Y. Xia, Angew. Chem. Int. Ed. 57 (2018) 2904–2908.
[111] J. Wang, L. Ji, X. Teng, Y. Liu, L. Guo, Z. Chen, J. Mater. Chem. A 7 (2019) 13149–13153.
[112] K. Wu, H. Li, S. Liang, Y. Ma, J. Yang, Angew. Chem. Int. Ed. 62 (2023) e202303563.
[113] S. Goodwin, D.A. Walsh, ACS Appl. Mater. Interfaces 9 (2017) 23654–23661.
[114] W. Li, N. Jiang, B. Hu, X. Liu, F. Song, G. Han, T.J. Jordan, T.B. Hanson, T.L. Liu, Y. Sun, Chem 4 (2018) 637–649.
[115] Y. Wang, L. Zhao, J. Ma, J. Zhang, Energy Environ. Sci. 15 (2022) 3830–3841.
[116] W. Yang, Y. Qiu, J. Bao, C. Luo, Q. Zhao, Ind. Eng. Chem. Res. 62 (2023) 9932–9938.
[117] V. Amstutz, K.E. Toghill, F. Powlesland, H. Vrubel, C. Comninellis, X. Hub, H.H. Girault, Energy Environ. Sci. 7 (2014) 2350–2358.
[118] P. Peljo, H. Vrubel, V. Amstutz, J. Pandard, J. Morgado, A. Santasalo-Aarnio, D. Lloyd, F. Gumy, C.R. Dennison, K.E. Toghilld, H.H. Girault, Green Chem. 18 (2016) 1785–1797.
[119] Y. Ji, F. Zhang, Mi. Zhou, J. Yu, Q. Wang, Int. J. Hydrogen Energy 45 (2020) 18888–18894.
[120] D. Frey, J. Kim, Y. Dvorkin, M.A. Modestino, Cell Rep. Phys. Sci. 1 (2020) 100226.
[121] M. Zhang, J. Guan, Y. Tu, S. Wang, D. Deng, The Innovation 2 (2021) 100144.
[122] P. Belleville, F. Guillet, A. Pons, J. Deseure, G. Merlin, F. Druart, J. Ramousse, E. Grindler, Int. J. Hydrogen Energy 43 (2018) 14867–14875.
[123] A. Ho, X. Zhou, L. Han, I. Sullivan, C. Karp, N.S. Lewis, C. Xiang, ACS Energy Lett. 4 (2019) 968–976.
[124] J. Wu, F. Lv, L. Pan, Y. Chen, ACS Sustain. Chem. Eng. 11 (2023) 17199–17205.
[125] J. Chen, R. Xiao, K. Fu, Y. Wu, Y. Guo, S. Yang, H. Li, J. Zheng, X. Li, Mater. Today 47 (2021) 16–24.
[126] I. Slobodkin, E. Davydova, M. Sananis, A. Breytus, A. Rothschild, Nat. Mater. (2024), https://doi.org/10.1038/s41563-023-01767-y.
[127] A.S. Cherevan, S.P. Nandan, I. Roger, R. Liu, C. Streb, D. Eder, Adv. Sci. 7 (2020) 1903511.
[128] J.-J. Chen, L. Vila-Nadal, A. Solé-Daura, G. Chisholm, T. Minato, C. Busche, T. Zhao, B. Kandasamy, A.Y. Ganin, R.M. Smith, I. Colliard, J.J. Carbó, J.M. Poblet, M. Nyman, L. Cronin, J. Am. Chem. Soc. 144 (2022) 8951–8960.
[129] W. Wu, X.-Y. Wu, S.-S. Wang, C.-Z. Lu, J. Catal. 378 (2019) 376–381.
[130] U. Brandt, Annu. Rev. Biochem. 75 (2006) 69–92.
[131] Q. Zhao, Z. Zhu, J. Chen, Adv. Mater. 29 (2017) 1607007.
[132] Q. Lei, B. Wang, P. Wang, S. Liu, J. Energy Chem. 38 (2019) 162–169.
[133] Y. Gao, G. Hong, B.-M. Yang, Y. Zhao, Chem. Soc. Rev. 52 (2023) 5541–5562.
[134] Y. Zhao, L. Zhang, X. Lia, Y. Shi, R. Ding, M. Teng, P. Zhang, C. Cao, P.J. Stang, Proc. Natl. Acad. Sci. U.S.A. 116 (2019) 4090–4098.
[135] J.D. Blakemore, R.H. Crabtree, G.W. Brudvig, Chem. Rev. 115 (2015) 12974–13005.
[136] P. Cieśla, P. Kocot, P. Mytych, Z. Stasicka, J. Mol. Catal. A Chem. 224 (2004) 17–33.
[137] T. Wu, K. Rajabimoghadam, A. Puri, D.D. Hebert, Y. Qiu, S. Eichelberger, M.A. Siegler, M. Swart, M.P. Hendrich, I. Garcia-Bosch, J. Am. Chem. Soc. 144 (2022) 16905–16915.
[138] B. You, X. Liu, N. Jiang, Y. Sun, J. Am. Chem. Soc. 138 (2016) 13639–13646.
[139] J. Zhang, X. Sheng, Z. Ding, H. Wang, L. Feng, X. Zhang, L. Wen, L. Jiang, X. Feng, Sci. Bull. 66 (2021) 164–169.
[140] L. Fan, Y. Ji, G. Wang, Z. Zhang, L. Yi, K. Chen, X. Liu, Z. Wen, J. Energy Chem. 72 (2022) 424–431.
[141] Q. Mao, W. Wang, K. Deng, H. Yu, Z. Wang, Y. Xu, X. Li, L. Wang, H. Wang, J. Energy Chem. 5 (2023) 58–66.
[142] Z.-X. Ge, Y. Ding, T.-J. Wang, F. Shi, P.-J. Jin, P. Chen, B. He, S.-B. Yin, Y. Chen, J. Energy Chem. 77 (2023) 209–216.
[143] X. Peng, S. Xie, S. Xiong, R. Li, P. Wang, X. Zhang, Z. Liu, L. Hu, B. Gao, P. Kelly, P.K. Chu, J. Energy Chem. 81 (2023) 574–582.
[144] F. Luo, S. Pan, Y. Xie, C. Li, Y. Yu, Z. Yang, J. Energy Chem. 90 (2024) 1–6.
[145] S. Kim, D. Kong, X. Zheng, J.H. Park, J. Energy Chem. (2024), https://doi.org/10.1016/j.jechem.2024.01.010.
[146] M. Hou, L. Chen, Z. Guo, X. Dong, Y. Wang, Y. Xia, Nat. Commun. 9 (2018) 438.
[147] Y. Feng, Q. Shi, J. Lin, E. Chai, X. Zhang, Z. Liu, L. Jiao, Y. Wang, Adv. Mater. 34 (2022) 2207747.
[148] L. MacDonald, B. Rausch, M.D. Symes, L. Cronin, Chem. Commun. 54 (2018) 1093–1096.
[149] A.D. Stergiou, D.H. Broadhurst, M.D. Symes, ACS Org. Inorg. Au 3 (2023) 51–58.
[150] L. Zhang, Y. Wang, Angew. Chem. Int. Ed. 62 (2023) e202219076.
[151] W. Lin, J. Lin, X. Zhang, L. Zhang, R. Borse, Y. Wang, J. Am. Chem. Soc. 145 (2023) 18141–18147.
[152] M. Potter, D.E. Smith, C.G. Armstrong, K.E. Toghill, EES Catal. 2 (2024) 379–388.